Bachelor Thesis

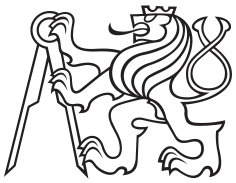

Czech Technical University in Prague

F4

Faculty of Nuclear Sciences and Physical Engineering
Department of Physics

Vortex curves in systems with point interactions

Filip Breuer

Supervisor: prof. RNDr. Pavel Exner, DrSc.
Field of study: Mathematical Engineering
Subfield: Mathematical physics
July 2023

FAKULTA JADERNÁ A FYZIKÁLNĚ INŽENÝRSKÁ

KATEDRA FYZIKY

ZADÁNÍ BAKALÁŘSKÉ PRÁCE

Akademický rok: 2022/2023

Student:	Filip Breuer
Studijní program:	Matematické inženýrství
Specializace:	Matematická fyzika
Název práce: (česky)	Vírové křivky v systémech s bodovými interakcemi
Název práce: (anglicky)	Vortex curves in systems with point interactions
Jazyk práce:	Angličtina

Pokyny pro vypracování:

1) Seznámit se s vlastnostmi hamiltoniánů popisujících kvantové systémy s bodovými interakcemi

2) Vyšetřit obecné vlastnosti vírových křivek v rozptylových řešeních příslušné Schrödingerovy rovnice a numerickou metodu jejich určení

3) Vyšetřit dvourozměrnou analogii daného rozptylového problému

4) Vyšetřit numericky rozptyl na konečně periodických strukturách

5) Pomocí Blochova rozkladu zformulovat obdobnou úlohu pro model nekonečného krystalu a zjistit, zda vírové křivky mohou být neuzavřené

Doporučená literatura:

[1] S. Albeverio, F. Gesztesy, R. Høegh-Krohn, H. Holden: Solvable Models in Quantum Mechanics, 2nd edition, AMS Chelsea 2005

[2] P. Exner, P. Šeba: Probability current tornado loops in three-dimensional scattering, Phys. Lett. A245 (1998), 35-39

Jméno a pracoviště vedoucího bakalářské práce:

prof. RNDr. Pavel Exner, DrSc.
Katedra fyziky, Fakulta jaderná a fyzikálně inženýrská ČVUT v Praze
Ústav jaderné fyziky AV ČR, v. v. i. - oddělení teoretické fyziky

Datum zadání bakalářské práce: 20.10.2022

Termín odevzdání bakalářské práce: 02.08.2023

Doba platnosti zadání je dva roky od data zadání.

ČESKÉ VYSOKÉ UČENÍ TECHNICKÉ V PRAZE
Fakulta jaderná a fyzikálně inženýrská
-3-

..... *garant studijního programu*

..... *vedoucí katedry*

..... *děkan*

V Praze dne 20.10.2022

ČESKÉ VYSOKÉ UČENÍ TECHNICKÉ V PRAZE
Fakulta jaderná a fyzikálně inženýrská

Břehová 7
115 19 Praha 1

PROHLÁŠENÍ

Já, níže podepsaný

Jméno a příjmení studenta:	Filip Breuer
Osobní číslo:	501476
Název studijního programu (oboru):	BMATIMF - Matematická fyzika

prohlašuji, že jsem bakalářskou práci s názvem:

Vírové křivky v systémech s bodovými interakcemi

vypracoval samostatně a uvedl veškeré použité informační zdroje v souladu s Metodickým pokynem o dodržování etických principů při přípravě vysokoškolských závěrečných prací.

V Praze dne 1. 7. 2023 ..... Breuer .....

podpis

Acknowledgements

I would like to thank prof. RNDr. Pavel Exner, DrSc. for guiding my work, as well as RNDr. Miloš Tater, CSc. for his help and advice on the programming part of this thesis.

A special thanks goes to my partner and my family. Your encouragement helped me overcome the most challenging parts of writing this thesis.

Abstract

In this thesis vortex curves in systems with periodically placed point interactions of equal strength are examined. The first part of the thesis deals with the necessary theory concerning this topic. Then a code in *Wolfram Mathematica 13.2* is set up to compute vortex curves numerically. This code is utilized to deal with the cases of a finite subset of points on the straight line, in the square lattice and in the (regular) hexagonal lattice. It has been found out that for some strength parameters of the point interactions and for certain range of deviations from the perpendicularly approaching particle ($8° \pm 0.5°$), the vortex curves form larger loops around all the point interactions. Moreover, in the case of the lattice, new vortex lines occur in front of and behind the lattice itself.

Keywords: vortex curves, point interaction, delta interaction, global effects

Supervisor: prof. RNDr. Pavel Exner, DrSc.
Katedra fyziky FJFI ČVUT a Oddělení teoretické fyziky ÚJF AV ČR

Abstrakt

V této bakalářské práci jsou zkoumány vírové křivky v periodických systémech bodových interakcí stejné síly. V první části práce je shrnuta teorii potřebná pro dané téma. Dále byl vytvořen kód v programu *Wolfram Mathematica 13.2* pro numerický výpočet vírových křivek. Z konečně periodických systémů byly ke zkoumání zvoleny konfigurace stejně vzdálených bodů na přímce, v čtvercové mřížce a pravidelné šestiúhelné mřížce. Díky kódu bylo zjištěno, že pro některé hodnoty síly bodových interakcí a do jisté odchylky od kolmého směru dopadu částice ($8° \pm 0.5°$) tvoří vírové čáry větší smyčky okolo všech interakcí. V případě mřížky se dokonce objevily vírové smyčky před, a za mřížkou samotnou.

Klíčová slova: vírové křivky, bodová interakce, delta interakce, globální jevy

Překlad názvu: Vírové křivky v systémech s bodovými interakcemi

Contents

Figures

Tables

Introduction

The present bachelor thesis deals with the vortex curves in systems with point interactions. The vortices are an important effect and they found their way into the different branches of physics, which shall be discussed in more detail in the following two sections. They appear in nonlinear differential equations – Navier-Stokes for fluids and Ginsburg-Landau for superfluids, however they also emerge in linear equations such as the Schrödinger equation, when describing scattering. We will show some results of scattering on a finitely periodic structures, described by means of the Schrödinger Hamiltonian of the type $H = -\Delta + \sum_{i=1}^{N} \lambda_i \delta_i(\cdot)$.

0.1 Vortices

In physics vortex means a circular motion of particles around a curve in some area of liquid. It is defined by the *vorticity* in the fluid, which indicates the tendency of the fluid to rotate, that can be defined as $\overrightarrow{v} \equiv \nabla \times \overrightarrow{u}$, where $\overrightarrow{u}$ is the velocity. We can distinguish vortices according to their shape - tornado, where the axis can be curved but it is not closed; and ring, where the axis is circular (i.e. closed). They are often observed in hydrodynamics.

Motion in hydrodynamics can be described by partial differential equations. Here we will focus on Newtonian fluids, i.e. those that obey Newton's law of viscosity, which is the simplest model of viscous fluids. This law puts in relation the strain rate ∇u (i.e. the rate of change of deformation over

time) and the viscous stress $\boldsymbol{\tau}$ (both 3×3 matrices) through constant (for a particular temperature) viscosity (fourth order) tensor $\boldsymbol{\mu}$

$$\boldsymbol{\tau} = \boldsymbol{\mu}(\nabla u). \tag{0.1.1}$$

In the case of an incompressible isotropic (mechanical properties are the same along all the axes) fluid, this equation simplifies into the following form

$$\tau = \mu \frac{du}{dx}. \tag{0.1.2}$$

As we can see, the strain rate, represented by the shear rate $\frac{du}{dx}$, and the stress, in the form of the shear stress τ, are in direct proportion with a scalar proportionality constant, the shear viscosity μ.

The motion of a Newtonian fluid can be described by the incompressible Navier-Stokes (N-S) equation

$$\frac{\partial \mathbf{u}}{\partial t} + (\mathbf{u} \cdot \nabla)\mathbf{u} - \nu \Delta \mathbf{u} = -\frac{1}{\rho}\nabla p + \mathbf{g}, \tag{0.1.3}$$

where p is the pressure, ρ is the mass density, $\mathbf{g}$ are external forces and ν is the kinematic viscosity defined as $\nu = \frac{\mu}{\rho}$ with μ being the dynamic viscosity. This equation is nonlinear. The time dependent solution $\mathbf{u}(t)$ is interpreted as the flow velocity and it is a vector field that for any point in the fluid and any time results in vector of velocity. The N-S equation is solvable only for some special cases, otherwise we have to apply numerical methods to find solutions. In addition, it is still unknown, whether there is always a smooth solution to this equation. In fact this belongs, together with six other questions, to the "Millennium Prize Problems" supported by the *Clay Mathematics Institute*.

If we simplify the N-S equation by taking the viscosity equal to zero, we will arrive at the incompressible Euler equations (E), which can be formulated in two forms – the convective form (= Lagrangian form)

$$\frac{D\rho}{Dt} = 0, \qquad \frac{D\mathbf{u}}{Dt} = -\frac{\nabla p}{\rho} + \mathbf{g}, \qquad \nabla \cdot \mathbf{u} = 0, \tag{0.1.4}$$

where we use notation from L-S. The first equation is the incompressible continuity equation and the third equation is the incompressibility constraint. The second form is called the conservation form (= Eulerian form)

$$\frac{\partial}{\partial t}\begin{pmatrix} \rho \\ \mathbf{j} \\ 0 \end{pmatrix} + \nabla \begin{pmatrix} \mathbf{j} \\ \frac{1}{\rho}\mathbf{j} \otimes \mathbf{j} + p\mathbb{I} \\ \frac{\mathbf{j}}{\rho} \end{pmatrix} = \begin{pmatrix} 0 \\ \mathbf{f} \\ 0 \end{pmatrix}, \tag{0.1.5}$$

where $\mathbf{j} = \rho\mathbf{u}$ is the momentum density, $\mathbf{f} = \rho\mathbf{g}$ is the force density and $\mathbb{I}$ is the identity matrix. Both of these forms are still nonlinear.

0.2 Quantum vortices

Vortices can also be observed in superfluids and superconductors (such as liquid helium and atomic gases), where they are called, in view of their properties, quantum vortices. In this case they are described as flux circulation.

Superfluid is a state of fluid with zero viscosity, so that the motion in the fluid is frictionless and therefore without any loss of kinetic energy. In the context of vortices, this would result in a vortex in a superfluid that would spin endlessly. Superfluidity occurs, for example, in helium (specifically in the isotopes ^{3}He, ^{4}He) when reaching very low temperatures [15].

Superconductors are materials, in which the electrical resistance suddenly changes to zero at a critical temperature, which is typical for each superconductor – compared to normal conductors, where the resistance gradually decreases as the temperature approaches the absolute zero. During the transition to its superconductive state, cooled below the critical temperature, the superconductor exhibits the Meissner effect, where all magnetic flux lines are expelled from the superconductor. Superconductors can be further divided into two groups, depending on how the Meissner state (the state in which none or just a small amount of magnetic field is inside) breaks down, when a strong magnetic field above the critical value H_{c_1} is applied. The type-I superconductors will suddenly break the Meissner state when the critical magnetic field strength is exceeded, whereas the type-II will change into the mix of ordinary and superconducting states, known as the *vortex state*, in which part of the magnetic flux pierces the superconductor. This process also features formation of magnetic field vortices called fluxons or Abrikosov vortices. As the strength of the field rises further, the material is being pierced by the magnetic flux more and more and the density of vortices increases until the second critical value H_{c_2} is reached and there the type-II superconductor changes from the mixed state into the state, where the Meissner effect is broken completely. A fluxon can be described as a small part of the material in the ordinary state surrounded by the superconducting state, where the supercurrents circulate around the part in the ordinary state. As discovered by B. S. Deaver, W. M. Fairbank [5] and R. Doll, M. Näbauer [6] independently in 1961, the magnetic flux crossing is then quantized.

In superfluids, we have a set of the Ginsburg-Landau (G-L) equations

$$\begin{aligned} \alpha\psi + \beta|\psi|^2\psi + \frac{1}{2m^*}(-i\hbar\nabla - e^*\mathbf{A})^2\psi = 0, \\ \nabla \times \mathbf{B} = \mu_0\mathbf{j}, \qquad \mathbf{j} = \frac{e^*}{m^*}\mathrm{Re}\{\psi^*(-i\hbar\nabla - e^*\mathbf{A})\psi\}, \end{aligned} \tag{0.2.1}$$

nonlinear equations describing the motion, where e^* is an effective charge and m^* is the effective mass – the mass which the particle appears to have when it responds to forces and interacts with other particles. $\mathbf{A}$ is the magnetic vector potential, which satisfies $\mathbf{A} = \nabla \times \mathbf{B}$, and $\mathbf{j}$ is the electric current density (without dissipation).

These G-L equations arise from the second-order phase transition, that Landau studied in 1930s [12], pursuing general theory of continuous (second-order) phase transitions.

The classification of the phase transitions was originally proposed by P. Ehrnfest and was based on the behaviour of the thermodynamic free energy, which depends on other thermodynamic variables. The order of the transition has been determined by the lowest derivative of the free energy that was not continuous at the transition (see for example [10]). Hence the terminology reflecting the behaviour of the first derivative: *discontinuous* $\equiv$ *first order* and *continuous* $\equiv$ *second order*. Later, the classification was reformulated, bearing the same names, to include other situations that did not fit into the original classification, such as the Ising model.

Landau's theory builds upon the premise that the free energy of system should obey symmetry of the Hamiltonian and that it should be analytic in the order parameter and its gradients. This allows us to rewrite the free energy in the vicinity of the critical temperature T_c as the Taylor expansion in the order parameter.

During the phase transition, the symmetry is often broken. This symmetry break can be parameterised by the order parameter, usually a real number. In some cases of the phase transition, for example superfluids and ferromagnetics, the parameter can be a complex number, a vector or a tensor, depending on the degree of freedom of the phase transition.

Ginsburg and Landau discussed the form of the order parameter for the superconductor and arrived at the complex field

$$\psi(r) = |\psi(r)|e^{i\phi(r)}. \tag{0.2.2}$$

$|\psi(r)|^2$ can be interpreted in the same way as in quantum mechanics – as a measure of the local superfluid density. Later there appeared additional interpretation as a fraction of electrons that have condensed into the superfluid state [8].

In both of the hydrodynamic equations (N-S, E), as well as in the superconductor equations (G-L) we can find vortices – solutions that have non-zero

vorticity. One of the few exactly solvable N-S equations, the Taylor-Green vortex [14], can serve us as an example in hydrodynamics. In the superconductors, vortices have been used by A. Abrikosov to explain the magnetic behavior of the type-II superconductors [1]. However, the study of vortices is not necessarily bound to nonlinear partial differential equations. Vortices can also be found in linear differential equations, such as a Schrödinger equation, when describing a scattering. This has been observed, for instance, in [4], [7], and it will be the subject of our investigation here.

Theoretical background

Chapter 1

Formulation

In this chapter we will describe the point interactions and some of their properties using the textbook [2].

1.1 The point interaction in 3D

In this thesis we consider a quantum mechanical description of a particle interacting with N scatters on potentials V_i, $i \in \{1, ..., N\}$, which can be described by the following Schrödinger Hamiltonian

$$H = -\Delta + \sum_{i=1}^{N} \lambda_i V_i, \tag{1.1.1}$$

where $\Delta = \left(\frac{\partial^2}{\partial x^2} + \frac{\partial^2}{\partial y^2} + \frac{\partial^2}{\partial z^2}\right)$ denotes the Laplace operator in $L^2(\mathbb{R}^3)$. If we take the potential in the form of a 3-dimensional Dirac's δ-function we get a formal Hamiltonian, which will be given a rigorous meaning later,

$$H = -\Delta + \sum_{i=1}^{N} \lambda_i \delta_i, \tag{1.1.2}$$

where $\delta_i(\mathbf{x}) = \delta(\mathbf{x} - \mathbf{x}_i)$, and $\mathbf{x}_{i,...,N} = (x_i, y_i, z_i)$ are N distinct points in $\mathbb{R}^3$ with a formal coupling constant $\lambda_i \in (-\infty, \infty]$, interpreted as the strength of the point source located at $\mathbf{x}_i$. The free particle case corresponds to $\lambda = 0$, although we will see that the same situation for the transformed *point interaction strength* α corresponds to $\alpha = \infty$. Resolvents of these

models can be expressed explicitly in terms of the locations and strengths of the sources. Such models appear in the literature under the names: "point interaction model", "zero-range potential model", "delta interaction model", "Fermi pseudopotential model" or "contact interaction model". A wider historical context of this theory can be found, for example, in [2].

1.2 One-centre point interaction

The treatment of the point-interaction model is based on the restriction to functions that vanish at the location of point interaction. For the negative Laplace operator, the domain is $\mathscr{D}(-\Delta) \coloneqq \{\psi \in L^2(\mathbb{R}^3) | -\Delta\psi \in L^2(\mathbb{R}^3)\} = H^2(\mathbb{R}^3)$, which is a Hardy space and here the Laplacian is self-adjoint. However, starting with the one-centre case

$$H = -\Delta + \lambda\delta(\cdot - y) \tag{1.2.1}$$

if we restrict the laplacian to the functions $f \in C_c^\infty(\mathbb{R}^3 \setminus \{y\})$, where

$$f \in C_c^\infty(X) \Leftrightarrow \begin{cases} f \in C^\infty(X) \\ supp(f) \coloneqq \overline{\{x \in X \,|\, f(x) \neq 0\}} \end{cases} \tag{1.2.2}$$

i.e. the set of smooth, compactly supported functions which vanish in the vicinity of the point y, we get $H_y = -\Delta|_{C_c^\infty(\mathbb{R}^3\setminus\{y\})}$, which is not self-adjoint anymore. Taking a closure $\dot{H}_y$ of H_y in $L^2(\mathbb{R}^3)$ (i.e. $\mathscr{D}(\dot{H}_y) = H_0^{2,2}(\mathbb{R}^3 \setminus \{y\})$, where $H^{m,n}$ denotes Sobolev spaces), we search for a self-adjoint extension of this operator, which we could identify with the formal Hamiltonian. According to [11] we can write its adjoint as

$$\dot{H}_y^* = -\Delta, \quad \mathscr{D}(\dot{H}_y^*) = \{g \in H^{2,2}_{\mathrm{loc}}(\mathbb{R}^3 \setminus \{y\}) \cap L^2(\mathbb{R}^3) \,|\, \Delta g \in L^2(\mathbb{R}^3)\},\ y \in \mathbb{R}^3. \tag{1.2.3}$$

The deficiency indices $n_\pm$ can be deduced from (1.2.4) with all of its assumptions, since they are defined as $n_\pm = \mathrm{dimKer}(\dot{H}_y^* \pm k^2)$. The unique solution of

$$\dot{H}_y^*\psi(k) = k^2\psi(k), \quad \psi(k) \in \mathscr{D}(\dot{H}_y^*), \quad k^2 \in \mathbb{C} \setminus \mathbb{R}, \quad \mathrm{Im}(k) > 0 \tag{1.2.4}$$

can be calculated and has the following form

$$\psi(k, x) = \frac{e^{ik|x-y|}}{|x-y|}. \tag{1.2.5}$$

Because of the requirement that the functions must belong to $L^2(\mathbb{R}^3)$, we arrive at one acceptable solution for each deficiency index, i.e. the deficiency indices are $(n_+, n_-) = (1, 1)$. From that it follows that $\dot{H}_y$ has a self-adjoint

extension [3]. With the help of the Theorem 1.2.2, we obtain a 1-parameter family of self-adjoint extensions

$$\begin{aligned}\mathscr{D}(H_{\theta,y}) &= \{g + c\psi_+ + ce^{i\theta}\psi_- \,|\, g \in \mathscr{D}(\dot{H}_y),\, c \in \mathbb{C}\},\\ H_{\theta,y}(g + c\psi_+ + ce^{i\theta}\psi_-) &= \dot{H}_y g + ic\psi_+ - ice^{i\theta}\psi_-, \qquad \theta \in [0, 2\pi), \quad y \in \mathbb{R}^3,\end{aligned} \tag{1.2.6}$$

where (including the normalisation constant)

$$\psi_\pm(x) = \frac{e^{i\sqrt{\pm i}|x-y|}}{4\pi|x-y|}, \qquad x \in \mathbb{R}^3 \setminus \{y\}, \quad \mathrm{Im}\sqrt{\pm i} > 0. \tag{1.2.7}$$

Then it is possible to implement spherical coordinates with the centre in y, in which we can decompose $L^2(\mathbb{R}^3)$ functions into the spherical (with S^2 being an unit sphere in $\mathbb{R}^3$) and the radial part

$$L^2(\mathbb{R}^3) = L^2((0,\infty); r^2dr) \otimes L^2(S^2). \tag{1.2.8}$$

With the use of the unitary transformation

$$U : L^2((0,\infty); r^2dr) \to L^2((0,\infty); dr), \qquad (Uf)(r) = rf(r), \tag{1.2.9}$$

it is possible to rewrite the radial part

$$L^2((0,\infty); r^2dr) = U^{-1}L^2((0,\infty); dr). \tag{1.2.10}$$

The basis for the spherical part consists of spherical harmonics $\{Y_{\ell,m} \,|\, \ell \in \mathbb{N}_0,\, m = 0, \pm1, ..., \pm\ell\}$. Using the notation where $[f_1, ..., f_n]$ is linear span of the vectors $f_1, ...f_n$, these two simplifications result in the following form of the decomposition

$$L^2(\mathbb{R}^3) = \bigoplus_{\ell=0}^{\infty} U^{-1}L^2((0,\infty); dr) \otimes [Y_{\ell,-\ell}, ...Y_{\ell,0}, ...Y_{\ell,\ell}]. \tag{1.2.11}$$

With respect to this decomposition, and with the help of unitary translation T_y to the centre y (i.e. $(T_yg)(x) = g(x+y)$, $g \in L^2(\mathbb{R}^3)$, $y \in \mathbb{R}^3$), we can rewrite $\dot{H}_y$

$$\begin{aligned}\dot{H}_y =& T_y^{-1}\left\{\bigoplus_{\ell=0}^{\infty} U^{-1}\dot{h}_\ell U \otimes \mathbb{1}\right\} T_y, \qquad y \in \mathbb{R}^3,\\ \dot{h}_\ell =& -\frac{d^2}{dr^2} + \frac{\ell(\ell+1)}{r^2}, \qquad r > 0, \quad \ell = 0, 1, 2, ...,\\ \mathscr{D}(\dot{h}_0) =& \{\phi \in L^2((0,\infty)) \,|\, \phi, \phi' \in AC_{\mathrm{loc}}((0,\infty));\, \phi(0_+) = \phi'(0_+) = 0;\\ & \phi'' \in L^2((0,\infty))\},\\ \mathscr{D}(\dot{h}_\ell) =& \{\phi \in L^2((0,\infty)) \,|\, \phi, \phi' \in AC_{\mathrm{loc}}((0,\infty));\\ & -\phi'' + \frac{\ell(\ell+1)}{r^2}\phi \in L^2((0,\infty))\}, \qquad \ell \geq 1,\end{aligned} \tag{1.2.12}$$

where $AC_{\mathrm{loc}}((0,\infty))$ denotes the set of absolutely continuous functions on $(0,\infty)$.

The unit operator $\mathbb{1}$ in the angular part is obviously self-adjoint. By standard results [13] $\dot{h}_\ell$, $\ell \geq 1$ are self-adjoint but the case for $\ell = 0$ requires additional examination. $\dot{h}_0$ has deficiency indices $(1,1)$ and can therefore be parameterized by a 1-parameter family of self-adjoint extensions $h_{0,\alpha}$

$$\begin{aligned} h_{0,\alpha} =& -\frac{d^2}{dr^2}, \\ \mathscr{D}(h_{0,\alpha}) =& \{\phi \in L^2((0,\infty)) | \phi, \phi' \in AC_{\mathrm{loc}}((0,\infty)); -4\pi\alpha\phi(0_+) + \phi'(0_+) = 0; \\ & \phi'' \in L^2((0,\infty))\}, \qquad -\infty < \alpha \leq \infty. \end{aligned} \tag{1.2.13}$$

Using $\tilde{g}(r) = rg(r)$, $\tilde{g} \in \mathscr{D}(\dot{h}_0)$, and substituting (1.2.7) into the linking condition at 0, where the δ-function is located in transformed coordinates (i.e. $\psi'(0_+) - \psi'(0_-) = \alpha\psi(0)$ generally and here restricted to the interval $[0,\infty)$ and thus effectively evaluating $\psi'(0_-) = 0$), we obtain

$$\begin{aligned} & 4\pi\alpha \left[\tilde{g}(r) + \frac{c}{4\pi} e^{i\sqrt{i}r} \frac{c}{4\pi} e^{i\theta} e^{i\sqrt{-i}r}\right]\Big|_{r=0_+} = \\ & = \frac{d}{dr}\left[\tilde{g}(r) + \frac{c}{4\pi} e^{i\sqrt{i}r} \frac{c}{4\pi} e^{i\theta} e^{i\sqrt{-i}r}\right]\Big|_{r=0_+} = \frac{c}{4\pi} e^{i\frac{3\pi}{4}} - e^{i\theta} e^{i\frac{\pi}{4}}, \end{aligned} \tag{1.2.14}$$

where the third equality evaluates the middle term of the equation. From this we have

$$\alpha = \frac{1}{4\pi} \cos\left(\frac{\pi}{4}\right)\left[\tan\left(\frac{\theta}{2}\right) - 1\right], \tag{1.2.15}$$

and finally we can write the 1-parameter family of self-adjoint extensions of $\dot{H}_y$ as

$$H_{\theta,y} = T_y^{-1}\left\{\left[U^{-1} h_{0,\alpha} U \oplus \bigoplus_{\ell=1}^{\infty} U^{-1}\dot{h}_\ell U\right] \otimes \mathbb{1}\right\} T_y. \tag{1.2.16}$$

The parameter α can be interpreted as a "renormalised coupling constant" λ in the one-point case of (1.1.1), i.e. as a strength parameter of the δ-function, where the case $\alpha = \infty$ leads to the case of the "free Hamiltonian" $H = -\Delta$. In this way we arrive at Theorem 1.2.1 describing self-adjoint extensions.

In the following section 1.2.1.2 we have theorems describing the resolvent (using Krein's formula 1.2.3) and domain, and in section 1.2.1.3, Theorem 1.2.6 describes some of the spectral properties of these extensions.

1.2.1 Properties of one-centre point interaction

Here we restate some useful theorems from the textbook [2].

1.2.1.1 Self-adjoint extensions

Summarizing the discussion above, we have the following theorem.

Theorem 1.2.1 ([2] - Th. I.1.1.1). *All self-adjoint extensions of $\dot{H}_y$ are given by*

$$-\Delta_{\alpha,y} = T_y^{-1}\left\{\left[U^{-1}h_{0,\alpha}U \oplus \bigoplus_{l=1}^{\infty} U^{-1}\dot{h}_l U\right]\otimes 1\right\}T_y, \qquad -\infty < \alpha \leq \infty, \quad y \in \mathbb{R}^3, \tag{1.2.17}$$

where $\dot{h}_l = -\frac{d^2}{dr^2} + \frac{l(l+1)}{r^2}$, $r > 0$, $l = 0, 1, 2, \ldots$, that are self-adjoint for $l \leq 1$, whereas $\dot{h}_0$ has deficiency indices (1,1) and U is a unitary transformation

$$U : L^2((0,\infty); r^2 dr) \longrightarrow L^2((0,\infty); dr), \qquad (Uf)(r) = rf(r). \tag{1.2.18}$$

All self-adjoint extensions $h_{0,\alpha}$ of $\dot{h}_0$ may be parameterized by

$$\begin{aligned} h_{0,\alpha} =& -\frac{d^2}{dr^2} \\ \mathscr{D}(h_{0,\alpha}) =& \{\phi \in L^2((0,\infty)) | \phi, \phi' \in AC_{loc}((0,\infty)); -4\pi\alpha\phi(0_+) + \phi'(0_+) = 0; \\ & \phi'' \in L^2((0,\infty))\}, \quad -\infty < \alpha \leq \infty. \end{aligned} \tag{1.2.19}$$

The special case $\alpha = \infty$ just leads to kinetic energy Hamiltonian $-\Delta$ (the Friedrichs extension of $\dot{H}_y$) in $L^2(\mathbb{R}^3)$

$$-\Delta_{\infty,y} = -\Delta \qquad on \qquad \mathscr{D}(-\Delta) = H^{2,2}(\mathbb{R}^3). \tag{1.2.20}$$

If $|\alpha| < \infty$, $-\Delta_{\alpha,y}$ describes a *point interaction* centred at $y \in \mathbb{R}^3$.

1.2.1.2 Basic properties of $-\Delta_{\alpha,y}$

Theorem 1.2.2 ([2] - Th. A.1). *Assume $\dot{A}$ to be densely defined, closed, symmetric operator in some Hilbert space $\mathscr{H}$ with deficiency indices $(1,1)$. If*

$$\dot{A}^*\phi(z) = z\phi(z), \qquad \phi(z) \in \mathscr{D}(\dot{A}^*), \quad z \in \mathbb{C} - \mathbb{R}, \tag{1.2.21}$$

then all self-adjoint extensions A_θ of $\dot{A}$ may be parameterized by a real parameter $\theta \in [0, 2\pi)$ where

$$\begin{aligned} \mathscr{D}(A_\theta) &= \{g + c\phi_+ + ce^{i\theta}\phi_- | g \in \mathscr{D}(\dot{A}), c \in \mathbb{C}\}, \\ A_\theta(g + c\phi_+ + ce^{i\theta}\phi_-) &= \dot{A}g + ic\phi_+ - ice^{i\theta}\phi_-, \qquad 0 \leq \theta < 2\pi, \end{aligned} \tag{1.2.22}$$

and

$$\phi_\pm = \phi(\pm i), \qquad ||\phi_+|| = ||\phi_-||. \tag{1.2.23}$$

Theorem 1.2.3 (Krein for deficiency indices 1, [2] - Th. A.2)**.** *Let B and C denote any self-adjoint extensions of $\dot{A}$, which is defined as in previous theorem. Then we have*

$$(B - z)^{-1} - (C - z)^{-1} = \lambda(z)(\phi(\bar{z}), \cdot)\phi(z), \qquad z \in \rho(B) \cap \rho(C), \tag{1.2.24}$$

where $\lambda(z) \neq 0$ for $z \in \rho(B) \cap \rho(C)$ and λ and ϕ may be chosen to be analytic in $z \in \rho(B) \cap \rho(C)$. In fact, $\phi(z)$ may be defined as

$$\phi(z) = \phi(z_0) + (z - z_0)(C - z)^{-1}\phi(z_0), \qquad z \in \rho(C), \tag{1.2.25}$$

where $\phi(z_0),\ z_0 \in \mathbb{C} - \mathbb{R}$, is a solution of

$$\dot{A}^*\phi(z) = z\phi(z), \qquad \phi(z) \in \mathscr{D}(\dot{A}^*), \quad z \in \mathbb{C} - \mathbb{R} \tag{1.2.26}$$

for $z = z_0$ and $\lambda(z)$ satisfies

$$\lambda(z)^{-1} = \lambda(z')^{-1} - (z - z')(\phi(\bar{z}), \phi(z')), \quad z, z' \in \rho(B) \cap \rho(C), \tag{1.2.27}$$

if $\phi(z)$ is chosen according to (1.2.25).

Theorem 1.2.4 ([2] - Th. I.1.1.2)**.** *The resolvent of $-\Delta_{\alpha,y}$ with one centre is given by*

$$\begin{aligned} (-\Delta_{\alpha,y} - k^2)^{-1} &= G_k + \left(\alpha - \frac{ik}{4\pi}\right)^{-1} (\overline{G_k(\cdot - y)}, \cdot)G_k(\cdot - y), \\ k^2 \in \rho(-\Delta_{\alpha,y}), &\quad Im(k) > 0, \quad -\infty < \alpha \leq \infty, \quad y \in \mathbb{R}^3, \end{aligned} \tag{1.2.28}$$

where

$$G_k = (-\Delta - k^2)^{-1}, \quad Im(k) > 0, \tag{1.2.29}$$

which in three dimensions has an integral kernel

$$G_k(x - x') = \frac{e^{ik|x-x'|}}{4\pi|x - x'|}, \quad Im(k) > 0, \quad x, x' \in \mathbb{R}^3, x \neq x'. \tag{1.2.30}$$

And the integral kernel of the resolvent of $-\Delta_{\alpha,y}$ has the form

$$\begin{aligned} (-\Delta_{\alpha,y} - k^2)^{-1}(x, x') &= \frac{e^{ik|x-x'|}}{4\pi|x - x'|} + \left(\alpha - \frac{ik}{4\pi}\right)^{-1} \frac{e^{ik|x-y|}}{4\pi|x - y|}\frac{e^{ik|y-x'|}}{4\pi|y - x'|}, \\ k^2 \in \rho(-\Delta_{\alpha,y}), &\quad Im(k) > 0, \quad x, x' \in \mathbb{R}^3, \quad x \neq x', \quad x \neq y, \quad , x' \neq y. \end{aligned} \tag{1.2.31}$$

Theorem 1.2.5 ([2] - Th. I.1.1.3). *The domain $\mathscr{D}(-\Delta_{\alpha,y})$, $-\infty < \alpha \leq \infty$, $y \in \mathbb{R}^3$, consists of all elements ψ of the type*

$$\psi(x) = \phi_k(x) + \left(\alpha - \frac{ik}{4\pi}\right)^{-1} \phi_k(y) G_k(x-y), \qquad x \neq y, \tag{1.2.32}$$

where $\phi_k \in \mathscr{D}(-\Delta) = H^{2,2}(\mathbb{R}^3)$ and $k^2 \in \rho(-\Delta_{\alpha,y})$, $Im(k) > 0$. The decomposition (1.2.32) is unique and with $\psi \in \mathscr{D}(-\Delta_{\alpha,y})$ of this form we obtain

$$(-\Delta_{\alpha,y} - k^2)\psi = (-\Delta - k^2)\phi_k. \tag{1.2.33}$$

Next, let $\psi \in \mathscr{D}(-\Delta_{\alpha,y})$ and assume that $\psi = 0$ in an open set $U \subseteq \mathbb{R}^3$. Then $-\Delta_{\alpha,y}\psi = 0$ in U.

1.2.1.3 Spectral properties of $-\Delta_{\alpha,y}$

Theorem 1.2.6 ([2] - Th. I.1.1.4). *Let $-\infty < \alpha \leq$, $y \in \mathbb{R}^3$. Then essential spectrum $\sigma_{ess}(-\Delta_{\alpha,y})$ is purely absolutely continuous and covers the nonnegative real axis*

$$\sigma_{ess}(-\Delta_{\alpha,y}) = \sigma_{ac}(-\Delta_{\alpha,y}) = [0,\infty), \quad \sigma_{sc}(-\Delta_{\alpha,y}) = \varnothing. \tag{1.2.34}$$

(Here σ_{ac} and σ_{sc} denote the absolutely and singularly continuous spectrum, respectively.)
If $\alpha < 0$, $-\Delta_{\alpha,y}$ has precisely one negative, simple eigenvalue, i.e. its point spectrum $\sigma_p(-\Delta_{\alpha,y})$ is given by

$$\sigma_p(-\Delta_{\alpha,y}) = \{-(4\pi\alpha)^2\}, \qquad -\infty < \alpha < 0, \tag{1.2.35}$$

with

$$4\pi(-\alpha)^{\frac{1}{2}} G_{-4\pi i\alpha}(x-y) = (-\alpha)^{\frac{1}{2}} \frac{e^{4\pi\alpha|x-y|}}{|x-y|}, \tag{1.2.36}$$

its strictly positive (normalized) eigenfunction. If $\alpha \geq 0$, $-\Delta_{\alpha,y}$ has no eigenvalues, i.e.

$$\sigma_p(-\Delta_{\alpha,y}) = \emptyset, \qquad 0 \leq \alpha \leq \infty. \tag{1.2.37}$$

1.2.2 Stationary scattering theory for one-centre point interaction

Thanks to the spherical symmetry we can apply a partial wave decomposition (1.2.17). Since for $l \geq 1$ $-\Delta_{\alpha,y}$ coincides with $-\Delta$, $-\Delta_{\alpha,y}$ describes an *s-wave*

interaction ($l = 0$, i.e. the solutions are independent of the angular variables). Thus we can focus mainly on the case $l = 0$.

If we define

$$\psi_{0,\alpha}(k,r) = \frac{1}{k}\sin(kr) + \frac{1}{4\pi\alpha - ik}e^{ikr}, \quad k \geq 0, \quad r \geq 0, \quad -\infty < \alpha \leq \infty. \tag{1.2.38}$$

By simple observation, we can see that the following relations hold true

$$\begin{aligned} &-4\pi\alpha\psi_{0,\alpha}(k,0_+) + \psi'_{0,\alpha}(k,0_+) = 0, \\ &-\psi''_{0,\alpha}(k,r) = k^2\psi_{0,\alpha}(k,r), \quad r > 0, \\ &\lim_{\varepsilon\to 0}\lim_{r'\to\infty}\frac{e^{-i(k+i\varepsilon)r'}}{h_{0,\alpha} - (k+i\varepsilon)^2}(r,r') = \psi_{0,\alpha}(k,r), \qquad k \geq 0, \quad r \geq 0, \\ &\qquad\qquad -\infty < \alpha \leq \infty. \end{aligned} \tag{1.2.39}$$

Consequently, $\psi_{0,\alpha}(k,r)$ constitute a set of generalised eigenfunctions associated with $h_{0,\alpha}$. Similarly,

$$\psi_l(k,r) = (\pi r)^{\frac{1}{2}}J_{l+\frac{1}{2}}(kr), \quad k \geq 0, \quad r \geq 0, \quad l = 1,2,..., \tag{1.2.40}$$

are generalised eigenfunctions of $\dot{h}_l$, $l = 1,2,...$, where J_ν denote Bessel functions of order ν. If we introduce the phase shift $\delta_{0,\alpha}(k)$ as

$$\cos[\delta_{0,\alpha}(k)] = \frac{4\pi\alpha}{\sqrt{(4\pi\alpha)^2 + k^2}}, \quad \sin[\delta_{0,\alpha}(k)] = \frac{k}{\sqrt{(4\pi\alpha)^2 + k^2}}, \quad k \geq 0, \quad -\infty < \alpha \leq \infty, \tag{1.2.41}$$

we can rewrite equation (1.2.38) into the following form

$$\psi_{0,\alpha}(k,r) = \frac{e^{i\delta_{0,\alpha}(k)}}{k}\sin[kr + \delta_{0,\alpha}(k)], \quad k > 0, \quad r \geq 0, \quad -\infty < \alpha \leq \infty. \tag{1.2.42}$$

From equations (1.2.40, 1.2.41) one can derive the on-shell partial wave scattering matrix

$$\begin{aligned} &\varphi_{0,\alpha}(k) = e^{2i\delta_{0,\alpha}(k)} = \frac{4\pi\alpha + ik}{4\pi\alpha - ik}, \quad k \geq 0, \quad -\infty < \alpha \leq \infty, \\ &\varphi_l(k) = 1, \quad \delta_l(k) = 0, \quad l = 1,2,... \end{aligned} \tag{1.2.43}$$

Now it is useful to compare it with the *effective range expansion* for real-valued spherically symmetric potentials V, obeying

$$\int_0^\infty re^{2ar}|V(r)|dr < \infty \qquad \text{for some} \quad a > 0. \tag{1.2.44}$$

Such an expansion is useful in the low-energy scattering and, in our case, reads

$$k^{2l+1}\cot[\delta_l(g,k)] = -\frac{1}{a_l(g)} + r_l(g)\frac{k^2}{2} + O(k^4), \quad k \geq 0, \quad g \in \mathbb{R}, \quad l = 0, 1, ..., \tag{1.2.45}$$

where the right-hand side is real analytic in k^2 near $k = 0$, and the $\delta_l(g,k)$ is by definition a phase shift associated with the Schrödinger operators $-\frac{d^2}{dr^2} + \frac{l(l+1)}{r^2} + gV(r)$. The coefficients $a_l(g)$ are the *partial wave scattering lengths* and $r_l(g)$, $l = 0, 1, ...,$ are the *effective range parameters*. From the explicit expressions of equation (1.2.45) for the point interaction (1.2.41)

$$k\cot[\delta_{0,\alpha}(k)] = 4\pi\alpha, \quad \delta_l(k) \equiv 0, \quad l = 1, 2, ..., \tag{1.2.46}$$

we can see that the effective range expansion is already exact in zeroth order with respect to k^2, i.e. the s-wave scattering parameters are given by

$$\begin{aligned} &a_{0,\alpha} = -\frac{1}{4\pi\alpha}, \\ &r_{0,\alpha} \equiv 0 \quad etc., \qquad -\infty < \alpha \leq \infty, \quad \alpha \neq 0, \end{aligned} \tag{1.2.47}$$

and all the low-energy parameters vanish in higher partial waves $l = 1, 2, ...$ This shows that the δ-interaction is indeed a zero-range interaction and acts (nontrivially) only in the s-wave $l = 0$. Moreover, it provides a physical interpretation of the boundary condition parameter $4\pi\alpha$ as the negative inverse scattering length.

Next let

$$\begin{aligned} &\Psi_{\alpha,y}(k\omega, x) = e^{ik\omega x} + \frac{e^{ik\omega y}}{(4\pi\alpha - ik)}\frac{e^{ik|x-y|}}{|x-y|}, \\ &k \geq 0, \quad \omega \in S^2, \quad -\infty < \alpha \leq \infty, \quad x, y \in \mathbb{R}^3, \quad x \neq y. \end{aligned} \tag{1.2.48}$$

Then, from the observation of the decomposition (1.2.17) and the wave function (1.2.38), $\Psi_{\alpha,y}(k\omega, x)$ is the scattering wave function corresponding to $-\Delta_{\alpha,y}$. Bessel function expansion of $e^{ik\omega|x-y|}$

$$\begin{aligned} &e^{ik\omega y}\Psi_{\alpha,y}(k\omega, x) = \frac{4\pi}{|x-y|}\Psi_{0,\alpha}(k|x-y|)\overline{Y_{00}(\omega)}Y_{00}(\omega_x) \\ &k \geq 0, \quad \omega \in S^2, \quad -\infty < \alpha \leq \infty, \quad x \neq y, \quad \omega_x = \frac{x}{|x|}. \end{aligned} \tag{1.2.49}$$

And again, by simple observation, $\Psi_{\alpha,y}(k\omega, x)$ fulfils

$$\begin{aligned} &-4\pi\alpha|x-y|\Psi_{\alpha,y}(k\omega, x) + \frac{x-y}{|x-y|}\nabla_x\Psi_{\alpha,y}(k\omega, x)|_{x=y} = 0, \\ &-(\nabla\Psi_{\alpha,y})(k\omega, x) = k^2\Psi_{\alpha,y}(k\omega, x), \qquad x \neq y, \\ &\lim_{\varepsilon\to 0}\lim_{\substack{|x'|\to\infty \\ \frac{|x'|}{x'}=-\omega}} 4\pi|x'|e^{-i(k+i\varepsilon)}\frac{|x'|}{-\nabla_{\alpha,y} - (k+i\varepsilon)^2}(x, x') = \Psi_{\alpha,y}(k\omega, x) \\ &\qquad\qquad k \geq 0, \quad \omega \in S^2, \quad -\infty < \alpha \leq \infty, \quad x \neq y. \end{aligned} \tag{1.2.50}$$

The *on-shell scattering amplitude* $f_{\alpha,y}(k,\omega,\omega')$ associated with $-\nabla_{\alpha,y}$ is then given by

$$f_{\alpha,y}(k,\omega,\omega') = \lim_{\substack{|x|\to\infty \\ \frac{|x|}{x}=\omega}} |x| e^{-ik|x|}[\Psi_{\alpha,y}(k\omega',x) - e^{ik\omega' x}] = \frac{e^{ik(\omega'-\omega)y}}{4\pi\alpha - ik}, \\ k \geq 0, \quad \omega,\omega' \in S^2, \quad -\infty < \alpha \leq \infty, \quad y \in \mathbb{R}^3, \tag{1.2.51}$$

and the corresponding *off-shell extension* $f_{\alpha,y}(k,p,q)$ is then defined as

$$f_{\alpha,y}(k,p,q) = \frac{e^{i(p-q)y}}{4\pi\alpha - ik} \\ k \in \mathbb{C}, \quad k \neq -4\pi i\alpha, \quad p,q \in \mathbb{C}^3, \quad -\infty < \alpha \leq \infty, \quad y \in \mathbb{R}^3, \tag{1.2.52}$$

and we get

$$f_{\alpha,y}(k,\omega,\omega') = f_{\alpha,y}(k,p,q)|_{|p|=|q|=k}, \\ p,q, \in \mathbb{R}^3, \quad \omega = \frac{p}{|p|}, \quad \omega' = \frac{q}{|q|}. \tag{1.2.53}$$

Finally, the unitary *on-shell scattering operator* $\mathscr{S}_{\alpha,y}(k)$ in $L^2(S^2)$ is

$$\mathscr{S}_{\alpha,y}(k) = 1 - \frac{k}{2\pi i}\frac{1}{4\pi\alpha - ik}(e^{-ik(\cdot)y},\cdot)e^{-ik(\cdot)y} \\ k \geq 0, \quad -\infty < \alpha \leq \infty, \quad y \in \mathbb{R}^3, \tag{1.2.54}$$

and for the choice of $y = 0$, it can be simplified to the form

$$\mathscr{S}_{\alpha,y}(k) = 1 + \frac{2ik}{4\pi\alpha - ik}(Y_{00},\cdot)Y_{00}. \tag{1.2.55}$$

1.3 Finite number of centers

Now let us focus on the multiple center problem

$$H = -\Delta + \sum_{i=1}^{N} \lambda_i \delta_i(\cdot - y_i). \tag{1.3.1}$$

In contrast to the one-centre case, here we meet a family of operators, for N given independent centres $Y = \{y_1, ..., y_N\}$, which is described below in Theorem 1.3.1.

From [9, Chapter 3] it follows, that there is a N^2-parameter family of self adjoint extensions of $-\Delta|_{\mathscr{D}_Y}$. However, we will only study the N-parameter family of extensions where the interaction is local. The resolvents of these operators are given by Krein's formula (Th. 1.3.2) and they can be written in the following form

$$\begin{gathered}(-\Delta_{\alpha,Y} - k^2)^{-1} = G_k + \sum_{j,\ell}^{N} [\Gamma_{\alpha,Y}]^{-1}_{j,\ell} (\overline{G_k(\cdot - y_j)}, \cdot) G_k(\cdot - y_\ell), \\ k^2 \in \rho(-\Delta_{\alpha,Y}), \quad \mathrm{Im}(k) > 0, \quad -\infty < \alpha \leq \infty, \quad y \in \mathbb{R}^3,\end{gathered} \tag{1.3.2}$$

with the same notation as in Theorem 1.2.4 and where $Y = \{y_1, ..., y_N\}$ are distinct points and

$$\Gamma_{\alpha,Y} = \left[\left(\alpha - \frac{ik}{4\pi} \right) \delta_{j,\ell} - G_k(y_j - y_\ell) \right]_{j,\ell}^{N}. \tag{1.3.3}$$

Due to the nature of the point interaction it is reasonable to expect locality of $-\Delta_{\alpha,Y}$ – in the sense that if $\psi = 0$ in $U \subset \mathbb{R}^3$, then also $-\Delta_{\alpha,Y}\psi = 0$ in U. Consequently, Theorem 1.3.3 gives us the domain $\mathscr{D}(-\Delta_{\alpha,Y})$ and it is a generalisation of Theorem 1.2.5 for the 1-centre case. We can see that $\mathscr{D}_Y \subseteq \mathscr{D}(-\Delta_{\alpha,Y})$ and that

$$-\Delta_{\alpha,Y}|_{\mathscr{D}_Y} = \Delta|_{\mathscr{D}_Y}, \tag{1.3.4}$$

which proves that $-\Delta_{\alpha,Y}$ is among the self-adjoint extensions from Theorem 1.3.1.

The essential spectrum of this operator $-\Delta_{\alpha,Y}$ is described in section 1.3.1.2.

1.3.1 Properties for N centers

Here we restate some useful theorems from the textbook [2].

Theorem 1.3.1 ([2] - Th. II.1.1.2). *The closed symmetric operator*

$$\dot{H}_Y = -\Delta|_{\mathscr{D}_Y}, \tag{1.3.5}$$

where

$$\mathscr{D}_Y = \{\psi \in H^{2,2}(\mathbb{R}^3) | \phi(y_j) = 0, y_j \in Y, j = 1, ...N\} \tag{1.3.6}$$

has deficiency indices (N, N) *and deficiency subspaces read*

$$\mathscr{K}_\pm = Ran(\dot{H}_Y \pm i)^\perp = [G_{\sqrt{\pm i}}(\cdot - y_1), ..., G_{\sqrt{\pm i}}(\cdot - y_N)], \quad Im(\pm i) > 0. \tag{1.3.7}$$

1.3.1.1 Basic properties of $-\Delta_{\alpha,Y}$

Theorem 1.3.2 (Krein for deficiency indices N>1, [2] - Th. A.3). *Let the* $\dot{A}$ *be a densely defined, closed, symmetric operator in* $\mathscr{H}$*, with deficiency indices* (N, N)*,* $N \in \mathbb{N}$ *and with two two self-adjoint extensions* B *and* C*. Denoting* $\mathring{A}$ *as a maximal common part of* B *and* C *[i.e.* $(\mathring{A} \subseteq B,\ \mathring{A} \subseteq C)(\forall A' | A' \subseteq B,\ A' \subseteq C)(A' \subseteq \mathring{A})$*]. And let* M*,* $0 < M \leq N$*, be the deficiency indices of* $\mathring{A}$ *and* $\{\phi_1(z), ..., \phi_M(z)\}$ *a corresponding span of subspace of* $\mathring{A}$*:*

$$\mathring{A}^* \phi_m(z) = z\phi_m(z), \qquad \phi_m(z) \in \mathscr{D}(\mathring{A}^*), \quad m = 1, ..., M, \quad z \in \mathbb{C} - \mathbb{R}, \tag{1.3.8}$$

and $\{\phi_1(z), ..., \phi_M(z)\}$ *are linearly independent. Then*

$$(B - z)^{-1} - (C - z)^{-1} = \sum_{m,n=1}^{M} \lambda_{m,n}(z)(\phi_n(\bar{z}), \cdot)\phi_m(z), \qquad z \in \rho(B) \cap \rho(C), \tag{1.3.9}$$

where matrix $\lambda(z)$ *is nonsingular for* $z \in \rho(B) \cap \rho(C)$ *and* $\lambda_{m,n}(z)$ *and* $\phi_m(z)$*,* $m, n = 1, ..., M$*, may be chosen to be analytic in* $z \in \rho(B) \cap \rho(C)$*. In fact,* $\phi_m(z)$ *may be defined as*

$$\phi_m(z) = \phi_m(z_0) + (z - z_0)(C - z)^{-1}\phi_m(z_0), \qquad m = 1, ..., M, \quad z \in \rho(C), \tag{1.3.10}$$

where $\phi_m(z_0),\ m = 1, ..., M,\ z_0 \in \mathbb{C} - \mathbb{R}$ *are linearly independent solutions of (1.3.8) for* $z = z_0$ *and the matrix* $\lambda(z)$ *satisfies*

$$[\lambda(z)]^{-1}_{mn} = [\lambda(z')]^{-1}_{mn} - (z - z')(\phi_n(\bar{z}), \phi_m(z')), \qquad m, n = 1, ..., M \quad z, z' \in \rho(B) \cap \rho(C), \tag{1.3.11}$$

if the $\phi_m(z),\ m = 1, ..., M$*, are defined according to (1.3.10).*

Theorem 1.3.3 ([2] - Th. II.1.1.3). *The domain $\mathscr{D}(-\Delta_{\alpha,Y})$, $y_j \in Y$, $-\infty < \alpha_j \leq \infty$, $j = 1, ..., N$, consists of all functions ψ of the type*

$$\psi(x) = \phi_k(x) + \sum_{j=1}^{N} a_j G_k(x - y_j), \qquad x \in \mathbb{R}^3 - Y, \tag{1.3.12}$$

where

$$a_j = \sum_{\ell=1}^{N} [\Gamma_{\alpha,Y}(k)]^{-1}_{j,\ell} \phi(y_\ell), \qquad j = 1, ..., N, \tag{1.3.13}$$

and $\phi_k \in \mathscr{D}(-\Delta) = H^{2,2}(\mathbb{R}^3)$ and $k^2 \in \rho(-\Delta_{\alpha,Y}), Im(k) > 0$. This decomposition is unique, and with ψ of this form we have

$$(-\Delta_{\alpha,Y} - k^2)\psi = (-\Delta - k^2)\phi_k. \tag{1.3.14}$$

Furthermore, let $\psi \in \mathscr{D}(-\Delta_{\alpha,Y})$ and assume $\psi = 0$ in an open set $U \subseteq \mathbb{R}^3$. Then $-\Delta_{\alpha,Y}\psi = 0$ in U.

1.3.1.2 Spectral properties of $-\Delta_{\alpha,Y}$

Theorem 1.3.4 ([2] - Th. II.1.1.4). *Let $y_j \in Y$, $-\infty < \alpha_j \leq \infty$, $j = 1, ..., N$. Then the essential spectrum of the operator $-\Delta_{\alpha,Y}$ is purely absolutely continuous and equals*

$$\sigma_{ess}(-\Delta_{\alpha,Y}) = \sigma_{ac}(-\Delta_{\alpha,Y}) = [0, \infty), \qquad \sigma_{sc}(-\Delta_{\alpha,Y}) = \varnothing. \tag{1.3.15}$$

Moreover,

$$\sigma_p(-\Delta_{\alpha,Y}) \subset (-\infty, 0) \tag{1.3.16}$$

and $-\Delta_{\alpha,Y}$ has at most N (negative) eigenvalues counting multiplicity. Let $Im(k) > 0$. Then

$$\begin{aligned} &k^2 \in \sigma_p(-\Delta_{\alpha,Y}) \Leftrightarrow \\ &\Leftrightarrow det[\Gamma_{\alpha,Y}(k)] = det\left[\left(\alpha_j - \frac{ik}{4\pi}\right)\delta_{j,\ell} - G_k(y_j - y_\ell)\right] = 0 \end{aligned} \tag{1.3.17}$$

and the multiplicity of the eigenvalue k^2 equals to the multiplicity of eigenvalue 0 of the matrix $\Gamma_{\alpha,Y}(k)$. Moreover, let $E_0 = k_0^2 < 0$ be an eigenvalue of $-\Delta_{\alpha,Y}$. Than the corresponding eigenfunctions ψ_0 are of the form

$$\psi_0(x) = \sum_{j=1}^{N} c_j G_{k_0}(x - y_j), \qquad Im(k_0) > 0, \tag{1.3.18}$$

where $(c_1, ..., c_N)$ are eigenvectors with eigenvalue zero of the matrix $\Gamma_{\alpha,Y}(k_0)$. If $-\Delta_{\alpha,Y}$ has a ground state it is nondegenerate and the corresponding eigenfunction can be chosen strictly positive (i.e. the associated eigenvector $(c_1, ..., c_N)$ fulfills $c_j > 0$, $j = 1, ..., N$).

1.3.2 Stationary scattering theory for N centers

Let

$$\begin{aligned}\Psi_{\alpha,Y}(k\omega,x) &= e^{ik\omega x} + \sum_{j,\ell=1}^{N} [\Gamma_{\alpha,Y}(k)]^{-1}_{j,\ell} e^{ik\omega y_\ell} \frac{e^{ik|x-y_j|}}{4\pi|x-y_j|}, \\ \det[\Gamma_{\alpha,Y}(k)] &\neq 0, \qquad k \geq 0, \quad \omega \in S^2, \quad \alpha_j \in \mathbb{R}, \\ & \qquad y_j \in Y, \quad j = 1,...,N, \quad x \notin Y,\end{aligned} \tag{1.3.19}$$

where $Y \subset \mathbb{R}^3$ is still a set of independent centres. Then $\Psi_{\alpha,Y}$ is formally of the form (1.3.12) with $\phi_k(x) = e^{ik\omega x}$, which is not in $L^2(\mathbb{R}^3)$ but satisfies

$$(-\Delta\phi_k)(x) = k^2\phi_k(x) \tag{1.3.20}$$

in the distributional sense. Furthermore,

$$(-\Delta\Psi_{\alpha,Y})(k\omega,x) = k^2\Psi_{\alpha,Y}(k\omega,x), \qquad x \notin Y, \tag{1.3.21}$$

and

$$\begin{aligned}&\lim_{\epsilon\to 0} \lim_{\substack{|x'|\to\infty \\ \frac{x'}{|x'|}=-\omega}} 4\pi|x'|e^{-i(k+i\varepsilon)|x'|} \left[-\Delta_{\alpha,Y} - (k+i\varepsilon)^2\right]^{-1}(x,x') = \Psi_{\alpha,Y}(k\omega,x), \\ &\det[\Gamma_{\alpha,Y}(k)] \neq 0, \quad k \geq 0, \quad \alpha_j \in \mathbb{R}, \quad y_j \in Y, \quad j = 1,..., \quad x \notin Y.\end{aligned} \tag{1.3.22}$$

And therefore the functions $\Psi_{\alpha,Y}$ constitute the generalized eigenfunctions of $-\Delta_{\alpha,Y}$ or, in other words, the scattering wave functions. With this in hand the *on-shell scattering amplitude* $f_{\alpha,Y}(k,\omega,\omega')$ associated with $-\Delta_{\alpha,Y}$ equals to

$$\begin{aligned}f_{\alpha,Y}(k,\omega,\omega') &= \lim_{\substack{|x|\to\infty \\ \frac{x}{|x|}=\omega}} |x|e^{-ik|x|}[\Psi_{\alpha,Y}(k\omega',x) - e^{ik\omega' x}] \\ &= \frac{1}{4\pi}\sum_{j,\ell=1}^{N} [\Gamma_{\alpha,Y}(k)]^{-1}_{j\ell} e^{ik(y_\ell\omega' - y_j\omega)}, \\ \det[\Gamma_{\alpha,Y}(k)] &\neq 0, \quad k \geq, \alpha_j \in \mathbb{R}, \quad y_j \in Y, \quad j = 1,...,N, \quad \omega,\omega' \in S^2.\end{aligned} \tag{1.3.23}$$

Hence the *off-shell extension* $f_{\alpha,Y}(k,p,q)$ of $f_{\alpha,Y}(k,\omega,\omega')$ reads

$$\begin{aligned}f_{\alpha,Y}(k,p,q) &= \frac{1}{4\pi}\sum_{j,\ell=1}^{N} [\Gamma_{\alpha,Y}(k)]^{-1}_{j\ell} e^{i(y_\ell q - y_j p)}, \\ \det[\Gamma_{\alpha,Y}(k)] &\neq 0, \quad k \in \mathbb{C}, \quad \alpha_j \in \mathbb{R}, \quad y_j \in Y, \quad j = 1,...,N, \quad p,q \in \mathbb{C}^3,\end{aligned} \tag{1.3.24}$$

so as to make

$$\begin{aligned}f_{\alpha,Y}(k,\omega,\omega') &= f_{\alpha,Y}(k,p,q)|_{|p|=|q|=k}, \\ p,q \in \mathbb{R}^3, \quad \omega &= \frac{p}{|p|}, \quad \omega' = \frac{q}{|q|}.\end{aligned} \tag{1.3.25}$$

Thus, the unitary *on-shell scattering operator* $\mathscr{S}_{\alpha,Y}(k)$ in $L^2(S^2)$ equals

$$(\mathscr{S}_{\alpha,Y}(k)\phi)(\omega) = \phi(\omega) - \frac{k}{2\pi i}\int_{S^2} f_{\alpha,Y}(k,\omega,\omega')\phi(\omega'), \qquad \phi \in L^2(S^2), \tag{1.3.26}$$

and with insertion of (1.3.23)

$$\begin{gathered}\mathscr{S}_{\alpha,Y}(k) = 1 - \frac{k}{8\pi^2 i}\sum_{j,\ell=1}^{N}[\Gamma_{\alpha,Y}(k)]^{-1}_{j,\ell}(e^{-iky_\ell(\cdot)},\cdot)e^{-iky_j(\cdot)} \\ \det[\Gamma_{\alpha,Y}(k)] \neq 0, \quad k \geq 0, \quad \alpha_j \in \mathbb{R}, \quad y_j \in Y, \quad j = 1,...,N.\end{gathered} \tag{1.3.27}$$

Nodal lines of various N-point configurations

Chapter 2

Models of various point interaction arrangements

2.1 Introduction

In quantum mechanics, the vortical behaviour is closely related to the phase ϕ of the wavefunction. If we take the wavefunction in the form $\psi(\mathbf{x}) = \sqrt{\rho(\mathbf{x})}e^{i\phi(\mathbf{x})}$, we can express the probability current as $\mathbf{j}(\mathbf{x}) = \rho(\mathbf{x})\nabla\phi(\mathbf{x})$ (using $\hbar = 2m = 1$). In the region with no external forces, the integral of $\mathbf{j}(\mathbf{r})$ over a closed loop can only be nonzero if it encircles a singularity in which the phase ϕ is ambiguous. However, since the solutions to the stationary Schrödinger equation are smooth functions, such singularities are $\psi = 0$ (these sets are called the nodal lines of the scattering wavefunction) [7]. The scattering wavefunctions often have nodal lines and they are in the forms of closed loops. The probability current in the vicinity of the nodal lines is locally cylindrical (tornado shaped) and thus it can be called *tornado type singularity*.

In this chapter we will have a look at models of scattering on the finite periodic structures of the point interactions. In these models we are interested in tornado type singularities of the corresponding wave function. Code to simulate such interactions has been made in *Wolfram Mathematica 13.2* and is available at `https://github.com/breuefil/VortexCurves.git`.

2.1.1 Mathematical problem in the background of the code

As we mentioned above, to find the nodal sets (i.e. the singularity points), we have to solve the following equation, using $\Psi_{\alpha,Y}(\mathbf{k},\cdot)$ as in (1.3.19) with the fixed momentum $\mathbf{k}$

$$\Psi_{\alpha,Y}(x,y,z)=0 \quad \Longleftrightarrow \quad \mathrm{Re}(\Psi_{\alpha,Y})(x,y,z)=0=\mathrm{Im}(\Psi_{\alpha,Y})(x,y,z). \tag{2.1.1}$$

From now on, the graphs of a plane section will use blue for the $\mathrm{Re}(\Psi_{\alpha,Y})(x,y,z)$ and orange for $\mathrm{Im}(\Psi_{\alpha,Y})(x,y,z)$ – an example with the direction of motion of the particle is shown in Fig. 2.1. We will use precision of 3 decimal places of the strength parameter to show where the nodal lines change, unless a higher precision is required.

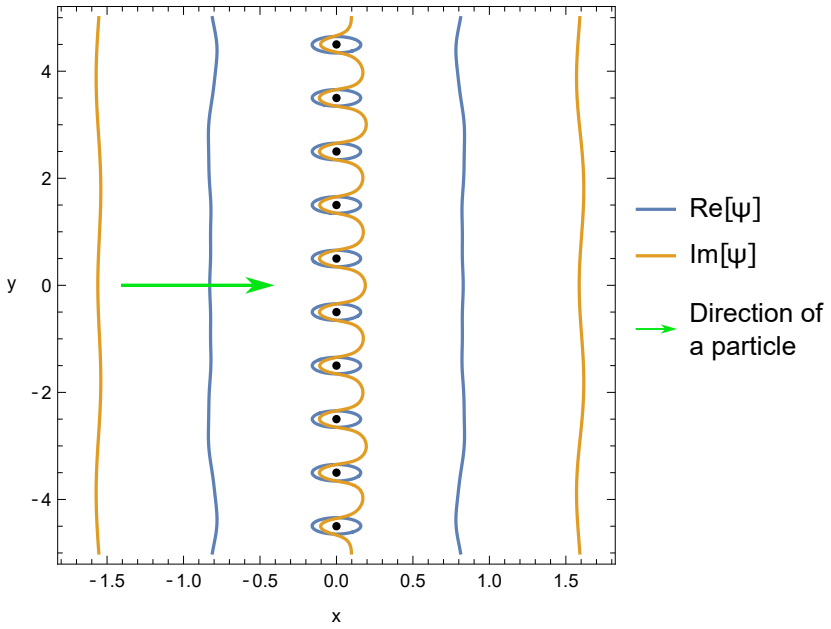

Figure 2.1: Perpendicular wave with equal point strengths $\alpha=-0.5$, wave momentum $\mathbf{k}=(2,0,0)$

2.2 Point interactions on the line

2.2.1 Perpendicular wave approaching 10 points on line

In this section we will simulate a 10-point interaction, where the points are equidistantly distributed on the y-axis (i.e. $y_j = (0, y_{j_2}, 0),\ j = 1, 2, ..., 10$) in points $y_{j_2} \in \{-\frac{9}{2}, -\frac{7}{2}, -\frac{5}{2}, -\frac{3}{2}, -\frac{1}{2}, \frac{1}{2}, \frac{3}{2}, \frac{5}{2}, \frac{7}{2}, \frac{9}{2}\}$ and the wave has a perpendicular momentum $\mathbf{k} = (k, 0, 0)$ to this *on the line* configuration of the point interactions. This configuration leads to a simplification of the N-point interaction scatter (1.3.19) into the form

$$\Psi_{\alpha,Y}(k, \mathbf{x}) = e^{ikx} + \sum_{j,\ell=1}^{10} [\Gamma_{\alpha,Y}(k)]^{-1}_{j,\ell} e^{iky_{\ell_1}} \frac{e^{ik|\mathbf{x}-\mathbf{y}_j|}}{4\pi|\mathbf{x}-\mathbf{y}_j|}, \tag{2.2.1}$$

with $\mathbf{x} = \{x, y, z\}$, $\mathbf{y}_j = \{y_{j_1}, y_{j_2}, y_{j_3}\}$, and where

$$\Gamma_{\alpha,Y}(k) := \left[\left(\alpha\frac{ik}{4\pi}\right)\delta_{j\ell} - \tilde{G}_k(\mathbf{y}_j - \mathbf{y}_\ell)\right]^{10}_{j,\ell=1}, \tag{2.2.2}$$

where $\tilde{G}_k(x)$ is the regularised Green's function

$$\tilde{G}_k(\mathbf{x}) = \begin{cases} \frac{e^{ik|\mathbf{x}|}}{4\pi|\mathbf{x}|}, & |\mathbf{x}| \neq 0, \\ 0, & |\mathbf{x}| = 0. \end{cases} \tag{2.2.3}$$

We choose the interaction strengths for all of the point interactions to be equal to α (i.e. $\alpha_j = \alpha,\ j = 1, 2, ..., 10$) and we are interested in the behaviour of the nodal lines depending on α. The wave momentum is chosen in this setting to be $\mathbf{k} = 2(1, 0, 0)$, i.e. with the magnitude $k = 2$, although it is logarithmically proportional to the interaction strength, so that the same results can be obtained with the transformed variables α and k and with transformed spacing of the point interactions.

In our simulation for $\alpha \leq -0.215$ nodal lines occurred around every point, as shown in the demonstrative case of $\alpha = -0.3$ in Fig. 2.2. With the growth of the strength parameter α, the number of nodal lines gradually decreases as the lines merge together until $\alpha = -0.166$, where there is only one line around all the points, and this state persists to $\alpha = -0.117$. Fig. 2.3 shows an example of this formation for $\alpha = -0.150$. From $\alpha = -0.116$, several nodal lines appear again and their number changes with the parameter α until $\alpha = 0.085$, where they disappear completely (Fig. 2.4).

All the changes in the number of loops are shown in Tab. 2.1. In this perpendicular case, the loops often (dis)appear in pairs, which is caused by

the reflection symmetry along the xz-plane. The interval of α for the given number of loops denotes the interval, including its extreme values, where the loop count does not change. Between the adjacent intervals, the change of a loop count occurs. This change, when two neighbouring loops merge or one loop splits into multiple loops, is accompanied by the effect that the "two" loops connect at one point and thus resembling figure 8 shape.

Interval of α	Loop count
(-∞, -0.215)	10
(-0.214, -0.181)	8
(-0.180, -0.1792)	6
(-0.1791, -0.1777)	5
(-0.1776, -0.167)	3
(-0.166, -0.117)	1
(-0.116, -0.068)	3
(-0.067, -0.053)	5
(-0.052, -0.031)	6
(-0.030, -0.018)	4
(-0.017, -0.016)	6
(-0.016, 0.0098)	5
(0.0099, 0.0108)	7
(0.0109, 0.0119)	9
(0.0120, 0.0122)	7
(0.0123, 0.130)	6
(0.131, 0.066)	4
(0.067, 0.084)	2
(0.085, ∞)	0

Table 2.1: Change of the number of loops for perpendicularly approaching wave with momentum $\mathbf{k} = (2, 0, 0)$, depending on α

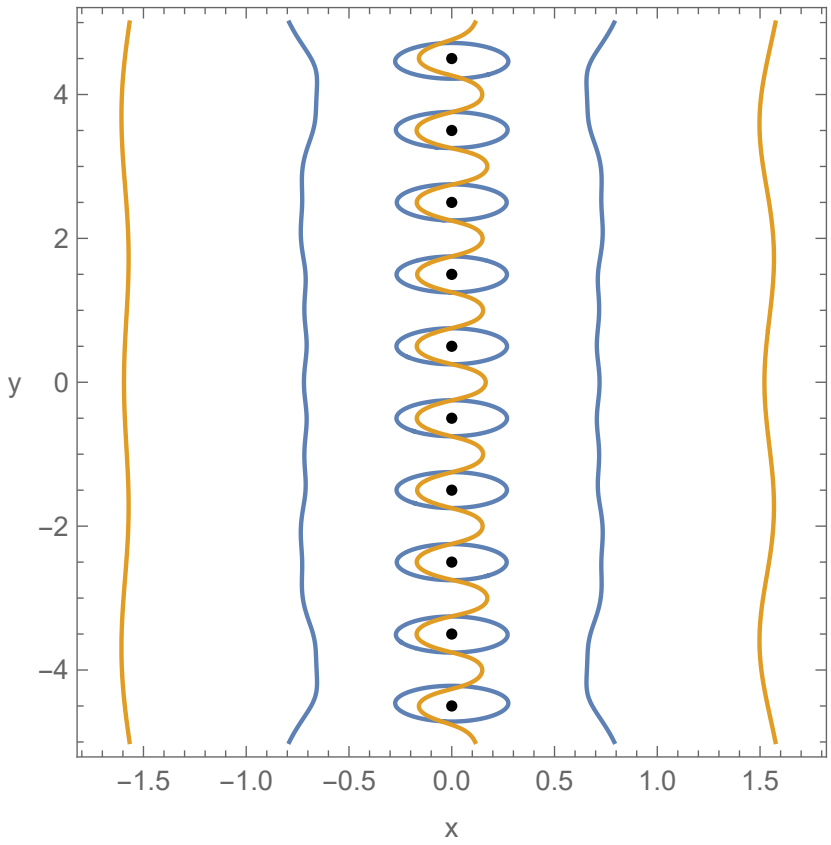

(a) Section by the z=0 plane

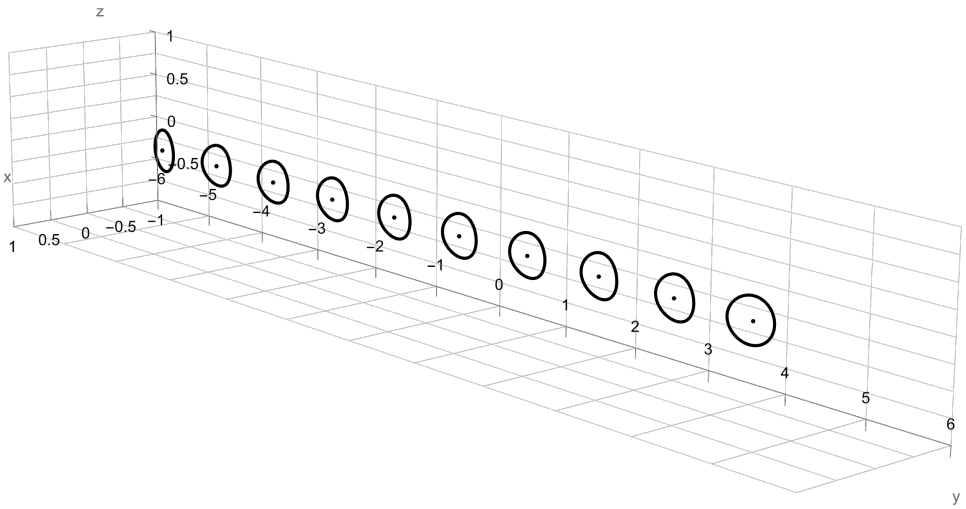

(b) Nodal lines

Figure 2.2: Nodal lines for the the strength parameter $\alpha = -0.3$, the same for all of the 10 interactions and for perpendicular wave with momentum $\mathbf{k} = (2, 0, 0)$

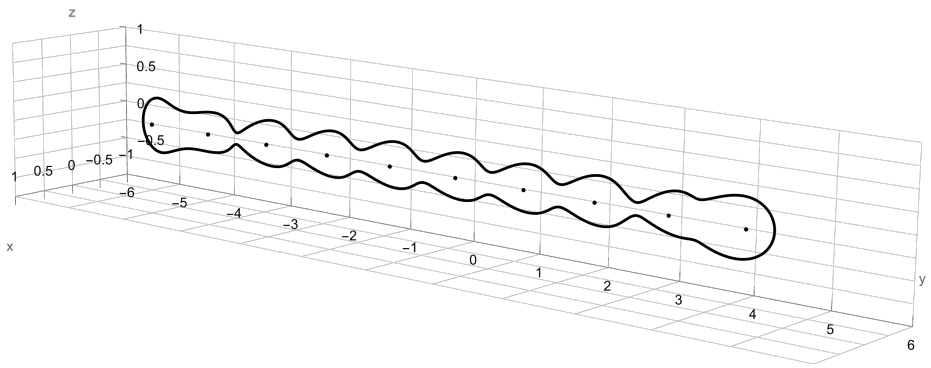

Figure 2.3: Nodal line for the strength parameter $\alpha = -0.150$, the same for all of the 10 interactions and for perpendicular wave with momentum $\mathbf{k} = (2, 0, 0)$

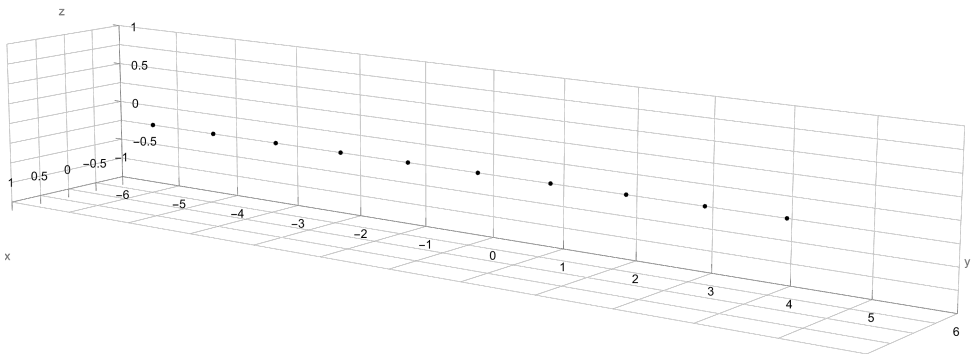

Figure 2.4: No nodal lines for the strength parameter $\alpha \geq 0.085$, the same for all of the 10 interactions and for perpendicular wave with momentum $\mathbf{k} = (2, 0, 0)$

2.2.2 Wave approaching 10 points on line at an angle

In this section, the setting is similar to that in section 2.2.1 except for the wave momentum $\mathbf{k} = k\omega$, where $\omega = (\omega_1, \omega_2, 0)$, $|\omega| = 1$, although other forms of ω could be used as well due to the rotational symmetry around the axis y. This assumption simplifies the scattering (1.3.19) into the following form

$$\Psi_{\alpha,Y}(\mathbf{k}, \mathbf{x}) = e^{ik(\omega_1 x + \omega_2 y)} + \sum_{j,\ell=1}^{N} [\Gamma_{\alpha,Y}(k)]^{-1}_{j,\ell} e^{ik(\omega y_{\ell_1} + \omega y_{\ell_2})} \frac{e^{ik|x-y_j|}}{4\pi|x-y_j|}. \quad (2.2.4)$$

2.2.2.1 45° angle

The first wave momentum setting we use is $\mathbf{k} = \sqrt{2}(1, 1, 0)$ (i.e. unit direction $\omega = \frac{1}{\sqrt{2}}(1, 1, 0)$ with a wave speed $k = 2$). Similarly as in the perpendicular case, for values lower than or equal to the critical interaction strength $\alpha_0 = -0.157$, we obtain a nodal line around each point interaction (Fig. 2.6).

Contrary to the perpendicular case, we did not observe merging of the loops into one loop around all of the points. Loops appeared and disappeared quite regularly until they disappeared completely for $\alpha = 0.192$. The complete process, which was identical to the perpendicular case in section 2.2.1, can be seen in Tab. 2.2.

To observe this behaviour, we will next examine small angle deviations from the perpendicular case in order to find an angle range where the global effect (a single loop around all of the point interactions) is present.

Interval of α	Loops
(-∞, -0.157)	10
(-0.156, -0.065)	9
(-0.064, -0.033)	8
(-0.032, -0.009)	7
(-0.008, -0.0077)	8
(-0.0076, -0.0074)	7
(-0.0073, -0.006726)	6
(-0.006725, -0.006720)	5
(-0.006719, -0.00670)	6
(-0.0066, -0.006316)	5
(-0.006315, -0.006304)	6
(-0.006303, -0.00629)	7
(-0.00628, -0.0060)	6
(-0.0059, -0.0052)	7
(-0.0051, -0.0048)	6
(-0.0047, -0.0044)	7
(-0.0043, 0.002)	6
(0.003, 0.009)	5
(0.010, 0.0117)	4
(0.0118, 0.0129)	5
⋮	⋮

Interval of α	Loops
(0.0130, 0.0137)	4
(0.0138, 0.016)	3
(0.017, 0.0171)	4
(0.0172, 0.0177)	3
(0.0178, 0.019)	2
(0.020, 0.023)	3
(0.024, 0.028)	2
(0.029, 0.032)	3
(0.033, 0.037)	2
(0.038, 0.0515)	3
(0.0516, 0.0519)	4
(0.0520, 0.055)	3
(0.056, 0.063)	4
(0.064, 0.071)	3
(0.072, 0.075)	2
(0.076, 0.099)	3
(0.100, 0.104)	4
(0.105, 0.134)	3
(0.135, 0.178)	2
(0.179, 0.191)	1
(0.192, ∞)	0

Table 2.2: Change of the *number of loops* (right column) for a case of wave approaching 10-point interactions on a y-axis at an 45° angle [i.e. in a direction given by $\mathbf{n} = (1, 1, 0)$], depending on α

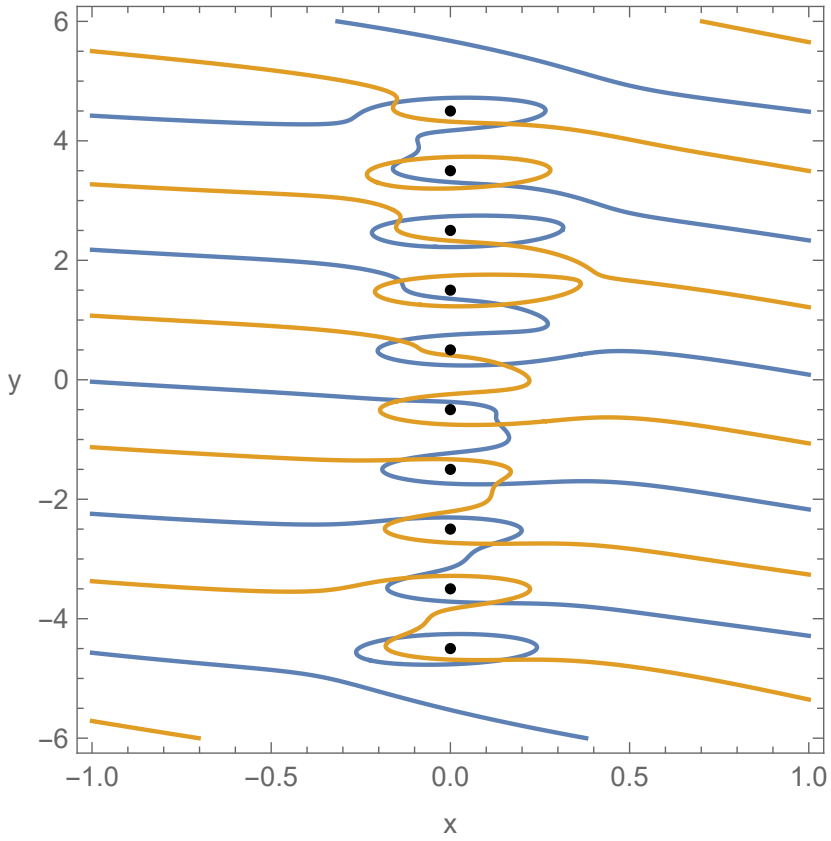

Figure 2.5: Real (blue) and imaginary (orange) part of $\psi = 0$ in the the z=0 plane, for wave with momentum $\mathbf{k} = \sqrt{2}(1, 1, 0)$ and interaction strength for all of the points $\alpha = -0.3$

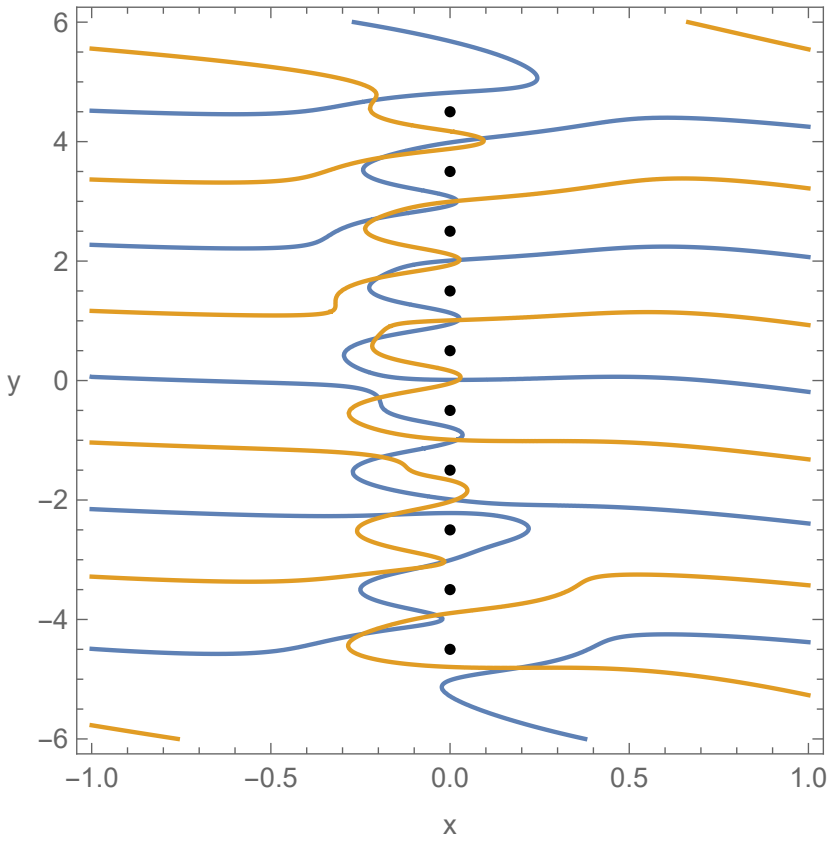

(a) Real (blue) and imaginary (orange) part of $\psi = 0$ in the the z=0 plane, for wave with momentum $\mathbf{k} = \sqrt{2}(1, 1, 0)$ and interaction strength for all of the points $\alpha = -0.3$ in the z=0 plane

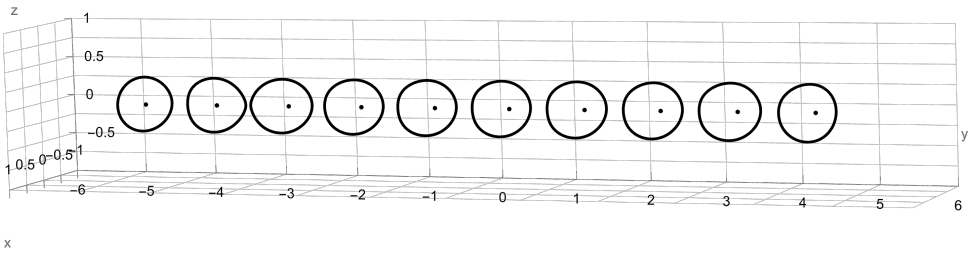

(b) Viewpoint 1

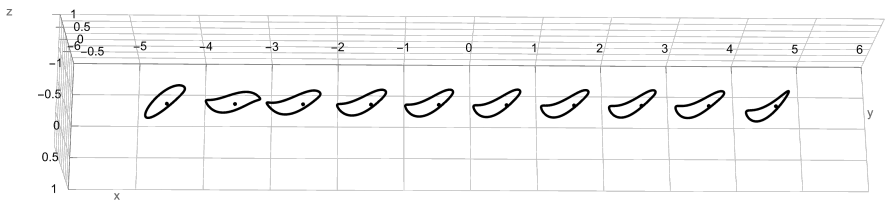

(c) Viewpoint 2

Figure 2.6: Nodal lines for the strength parameter $\alpha = -0.16$, the same for all of the 10 interactions and for wave with momentum $\mathbf{k} = \sqrt{2}(1, 1, 0)$

2.2.2.2 1° deviation from perpendicular case

Let us start from the deviation of approximately 1° from the perpendicular case in the xy-plane, specifically

$$k = 2, \qquad \Omega = (1, 0.0175, 0), \qquad \omega = \frac{\Omega}{||\Omega||}, \qquad ||\omega|| = 1. \tag{2.2.5}$$

Here for $\alpha \leq -0.216$ there is a loop around each point. For $\alpha = -0.215$ there are only 9 loops present. Gradually, as α increases, the number of loops decreases (sometimes a new loop can appear, but in general the number of loops decreases), until we arrive at $\alpha = -0.165$, where, again as in the case of perpendicular wave, we have only one loop encircling all of the points. A representative example is shown in the set of figures 2.7. This state remains until $\alpha = -0.120$, and from $\alpha = -0.119$ the number of loops increases and then again declines, similar to the evolution in the perpendicular wave (Tab. 2.1). Finally for $\alpha = 0.085$ the nodal lines vanish completely.

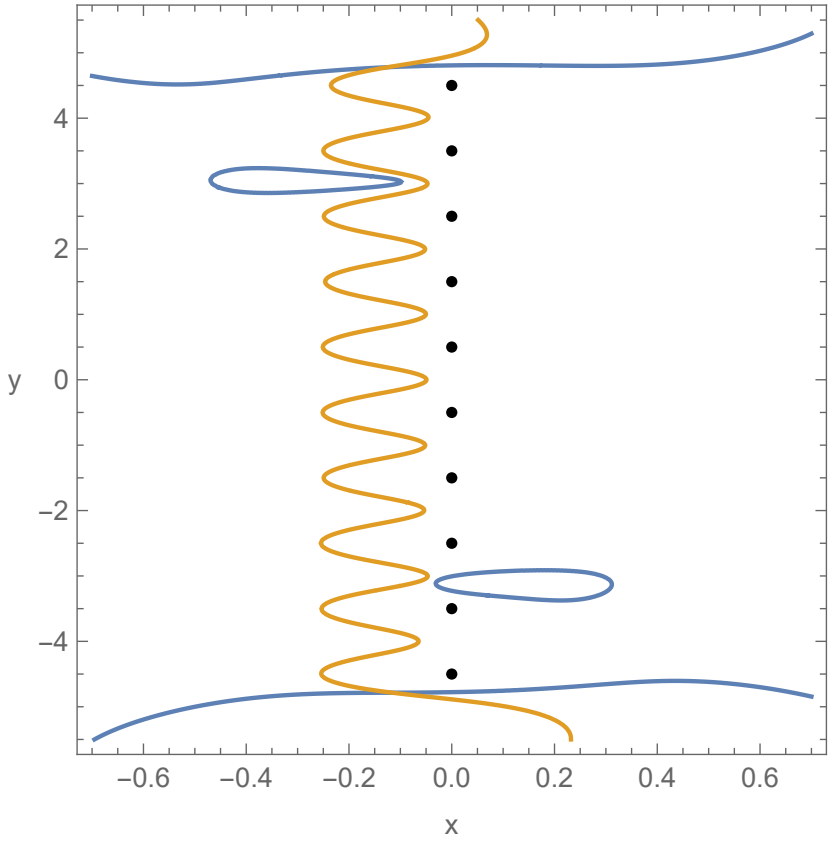

(a) Section by the z=0 plane

Figure 2.7: Real (blue) and imaginary (orange) part of $\psi = 0$ in the z=0 plane, for the strength parameter $\alpha = -0.15$, the same for all of the 10 interactions and for a wave with momentum direction Ω=(1,0.0175,0), normalised to $k = 2$

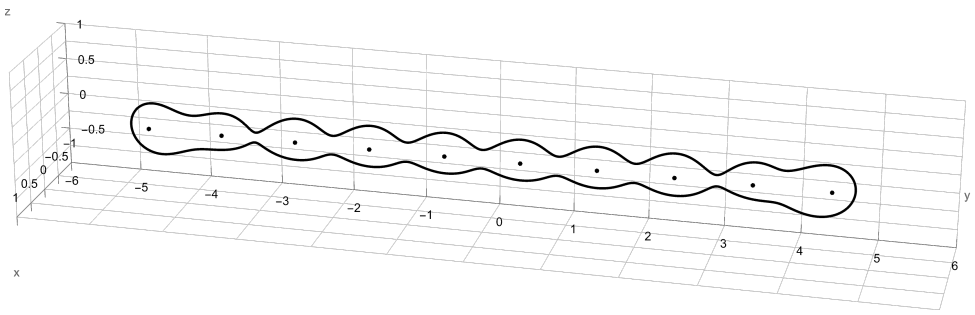

(b) Viewpoint 1

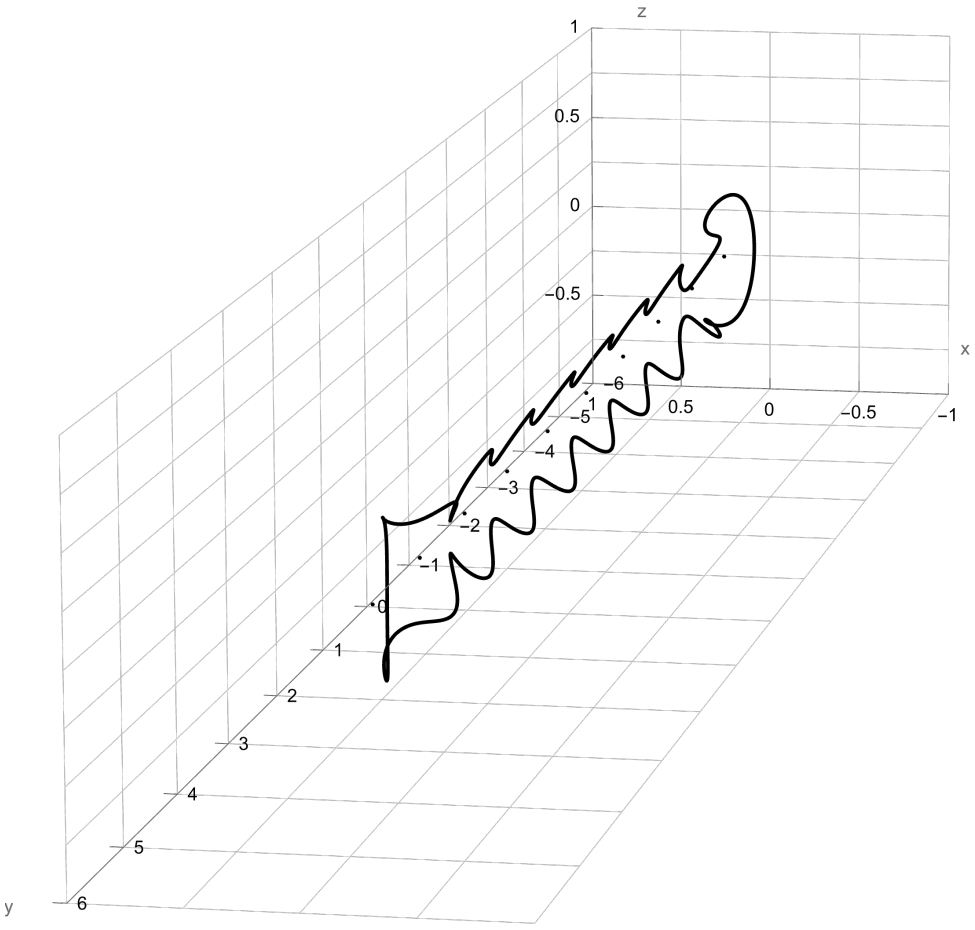

(c) Viewpoint 2

Figure 2.7: Nodal lines for the strength parameter $\alpha = -0.15$, the same for all of the 10 interactions and for wave with momentum direction Ω=(1,0.0175,0), normalised to $k = 2$

2.2.2.3 8° deviation from the perpendicular wave

We have the following setting

$$k = 2, \qquad \Omega = (1, 0.14, 0), \qquad \omega = \frac{\Omega}{||\Omega||}, \qquad ||\omega|| = 1, \tag{2.2.6}$$

which corresponds to a deviation from the perpendicular case of about 8° in the xy-plane. For $\alpha \leq -0.217$ there is a loop around each point. For $\alpha = -0.216$, there are only 9 loops. Gradually decreasing the number of loops we get to $\alpha = -0.152$ where we have only one loop encircling all of the points (Fig. 2.8). This state remains until $\alpha = -0.144$, for $\alpha = -0.143$ we observe that two loops merge into one, forming for a moment an 8 like figure, and from $\alpha = -0.132$ the number of loops increases, and than declines, similarly to the perpendicular wave (Tab. 2.1). Finally for $\alpha = 0.114$ the nodal lines vanish completely.

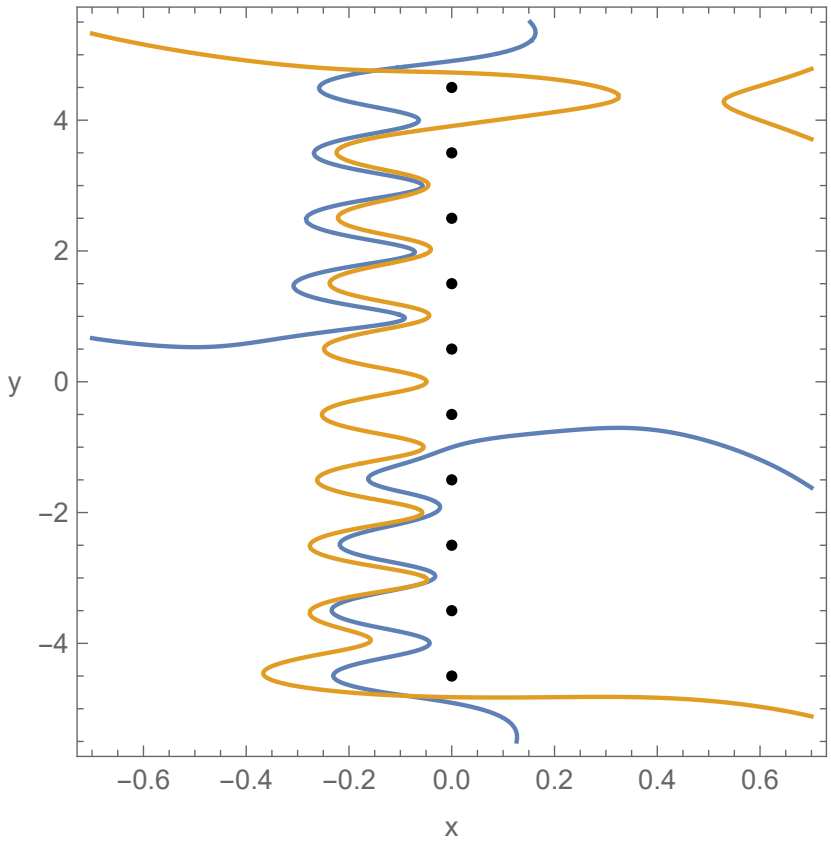

(a) Section by the z=0 plane

Figure 2.8: Real (blue) and imaginary (orange) part of $\psi = 0$ in the z=0 plane, for the strength parameter $\alpha = -0.15$, the same for all of the 10 interactions and for a wave with momentum direction Ω=(1,0.14,0), normalised to $k = 2$

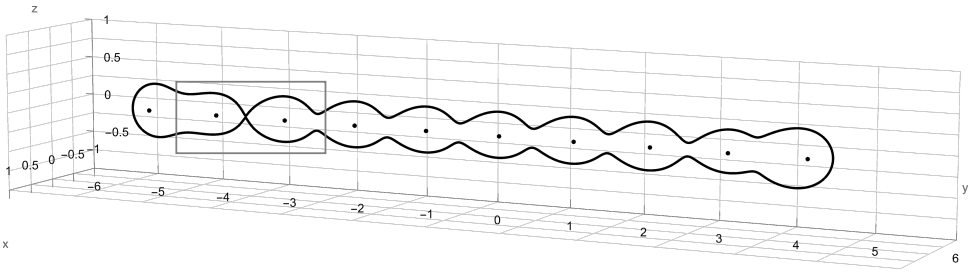

(b) Section by the z=0 plane

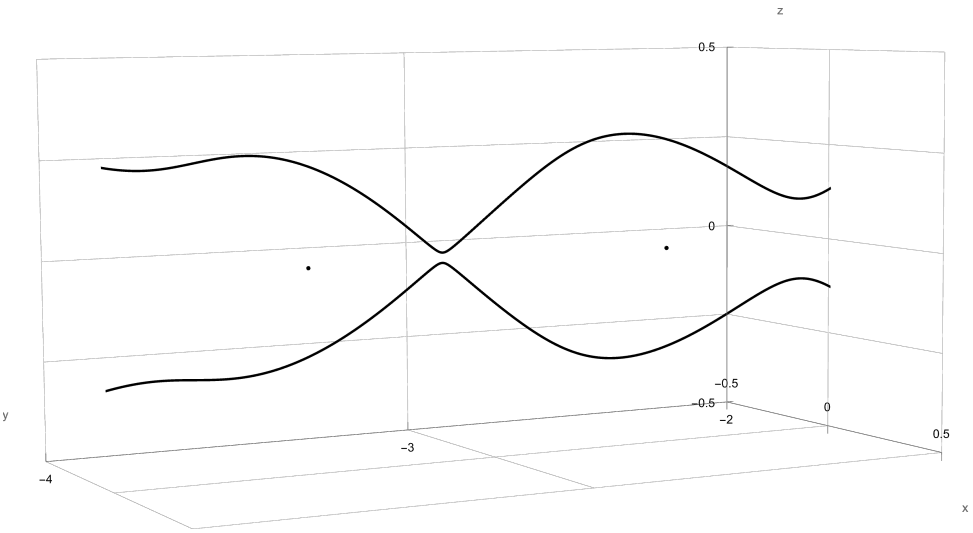

(c) Loops

Figure 2.8: Nodal lines for the strength parameter $\alpha = -0.15$, the same for all of the 10 interactions and for wave with momentum direction Ω=(1,0.14,0), normalised to $k = 2$

2.2.2.4 8.5° deviation from the perpendicular wave

We have the following setting

$$k = 2, \qquad \Omega = (1, 0.15, 0), \qquad \omega = \frac{\Omega}{||\Omega||}, \qquad ||\omega|| = 1, \tag{2.2.7}$$

which corresponds to a deviation from the perpendicular case of about 8.5° in the xy-plane. For $\alpha \leq -0.215$ there is a loop around each point. For $\alpha = -0.214$ two loops merge together and thus we only have 9 loops. Gradually, as we increase the value of α, we get a decreasing number of loops. In the interval where we previously observed one loop around all of the points, however, we now get two loops instead. That means we do not observe this global effect. Specifically two loops appeared from $\alpha = -0.161$ to $\alpha = -0.087$ (Fig. 2.9). From $\alpha = -0.086$ the number of loops increases again and then finally declines to the point of $\alpha = 0.085$, where the nodal lines vanish completely.

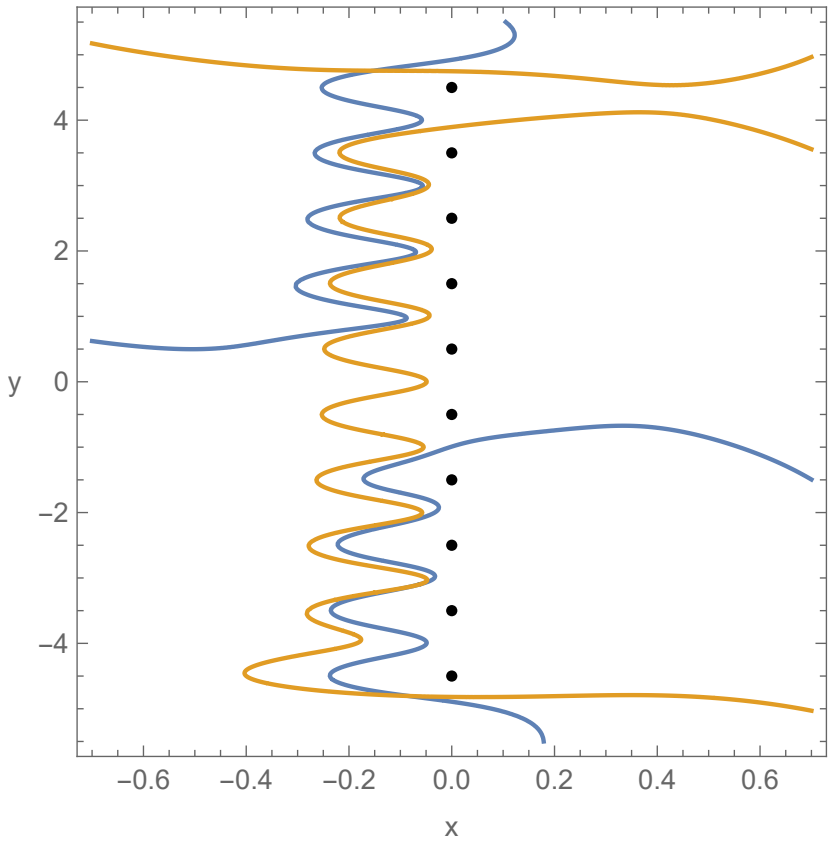

(a) Section by the z=0 plane

Figure 2.9: Real (blue) and imaginary (orange) part of $\psi = 0$ in the z=0 plane, for the strength parameter $\alpha = -0.15$, the same for all of the 10 interactions and for a wave with momentum direction Ω=(1,0.15,0), normalised to $k = 2$

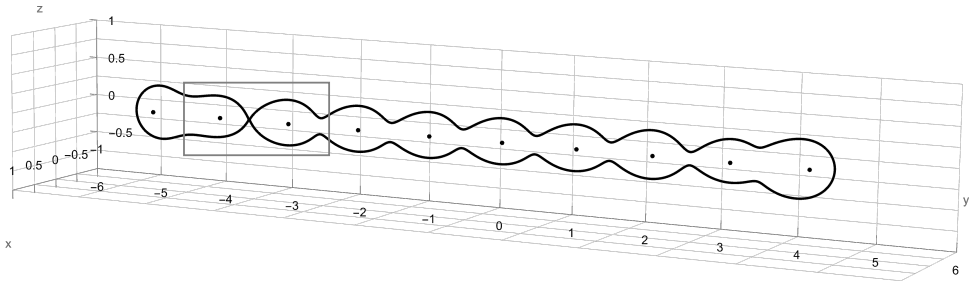

(b) Loops

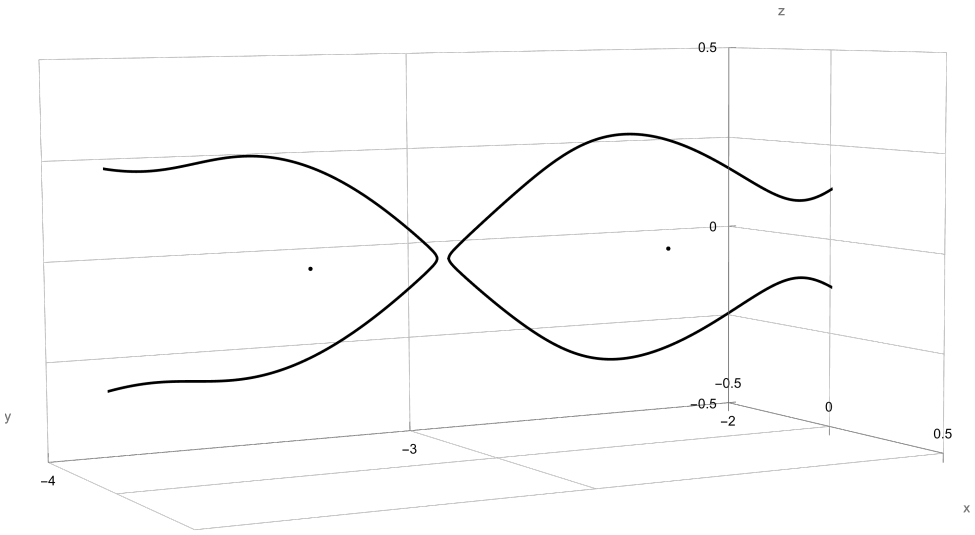

(c) Close-up

Figure 2.9: Nodal lines for the strength parameter $\alpha = -0.15$, the same for all of the 10 interactions and for wave with momentum direction Ω=(1,0.15,0), normalised to $k = 2$

2.2.3 Summary for 10 point interactions on the line

In this section, we first examined a wave approaching 10 point interactions on the line perpendicularly (section 2.2.1). For a certain interval of strength of the interactions $\alpha \in (-0.166, -0.117)$ (for our configuration with momentum $\mathbf{k} = 2(1, 0, 0)$ and spacing of 1 between the adjacent points) we observed one "global line" surrounding all of the point interactions (instead of nodal line around each point interaction). From the shape of the global line we conjecture, that in the infinite case, the global effect would take the form of two (almost straight) lines above and below (positive and negative z respectively) the points. For this assumption to be confirmed, however, we would have to use different methods.

Subsequently we investigated (section 2.2.2) whether this global effect also appears for a small angular deviation from the perpendicular wave, where we originally noticed this effect. Starting with a deviation of about 1°, we discovered that the effect holds. During further investigation, we conclude that this effect occurs for deviations up to 8° ($\pm$ 0.5°). This deviation emerges only from the results where we observed the effect and where we did not, and it does not include, for example, errors arising from the code construction.

2.3 Point interactions forming a square lattice

In this section we will investigate another periodic structure, a plane square lattice, that will be perpendicular to the momentum of the particle. Here we want to choose a sufficiently large periodic structure to approximate an infinite case, a $\mathbf{n} \times \mathbf{n}$ lattice. The point interactions will be equidistantly arranged in $\mathbf{n}$ rows, each for constant height $z_\zeta = \zeta$, $\zeta = -\frac{\mathbf{n}-1}{2}, -\frac{\mathbf{n}-1}{2}+1, ..., 0, 1, ..., \frac{\mathbf{n}-1}{2}$. Each row will contain $\mathbf{n}$ point interactions with y-coordinate $y_\eta = \eta$, $\eta = -\frac{\mathbf{n}-1}{2}, -\frac{\mathbf{n}-1}{2}+1, ..., 0, 1, ..., \frac{\mathbf{n}-1}{2}$, all with x-coordinate $x = 0$. The wave momentum for all waves in this section will be normalised to 2 (i.e. $||\mathbf{k}|| = 2$), same as in the previous sections.

2.3.1 Wave perpendicular to 25 points forming a square lattice

Let us start with a wave that approaches the 5×5 grid perpendicularly, with momentum $\mathbf{k} = 2(1, 0, 0)$. Again, we will arrive at simplification (2.2.1) as in section 2.2.1.

Similarly to the perpendicular wave approaching the points on a line (section 2.2.1), loops around each point interaction occur until certain strength of the interactions is acquired (here $\alpha \leq -0.320$), and then they start to merge together. Nevertheless, in this particular case we observed that they are accompanied by additional nodal lines outside of the lattice (with respect to the x-axis). In the next step we investigated these loops in more detail.

The state, where there are loops only locally around point interactions occurs for $\alpha \leq -0.620$. Subsequently four additional loops appear. Three of them are located in front of the lattice (at $x \approx -3$, at $x \approx -1.5$, at $x \approx -4.8$) and one of them is behind it (at $x \approx 4$) (with respect to the direction of the spatial wave), for $\alpha = -0.619$, $\alpha = -0.554$, $\alpha = -0.398$ and for $\alpha = -0.487$ respectively. These configurations are illustrated in Figs. 2.10, 2.11.

This configuration of the "outside loops" holds until the strength parameter $\alpha = -0.319$. For $\alpha = -0.318$ the closest loop in front of the lattice (with respect to the direction of the spatial wave) merges with certain loops around the point interactions (Fig. 2.12).

From $\alpha = -0.329$ the loops around each of the point interactions begin to merge together, starting with the loops in the corners. A global effect, when loops "in the lattice" form larger loops, occurs for $\alpha \in (-0.152,\ -0.107)$, with only two loops around the lattice remaining (Fig. 2.13). The last remaining loop outside the lattice at $x \approx -1.7$ (that appeared for $\alpha = -0.487$ at $x \approx -1.5$ and with the growth of α slightly moved) disappears for $\alpha = 0.109$. Finally, for $\alpha = 0.208$, the last loop in the lattice (which is also the last in the configuration) disappears and thus there are no nodal lines for $\alpha \geq 0.208$.

Some significant changes, described above, can be found in the Tab. 2.3 below.

Interval of α	Nodal line change
(-∞, -0.620)	Loops are only around each nodal point
-0.619	Additional loop at $x \approx -3$ appears
-0.554	Additional loop at $x \approx +4$ appears
-0.487	Additional loop at $x \approx -1.5$ appears
-0.398	Additional loop at $x \approx -4.8$ appears
-0.329	Loops around points start merging together
(-0.319, -0.318)	Loop in front of lattice merges with loop around lattice
(-0.153, -0.152)	Loop in the middle of lattice disappears
(-0.107, -0.106)	Loops around lattice split into smaller loops
(0.108, 0.109)	Last loops outside of lattice disappear ($x \approx -1.7$)
(0.207, 0.208)	Last loops in lattice disappear
(0.208, ∞)	No nodal lines

Table 2.3: Some significant changes of nodal line configuration for 25-point interaction, square lattice perpendicularly approaching wave with momentum $\mathbf{k} = (2, 0, 0)$, depending on α

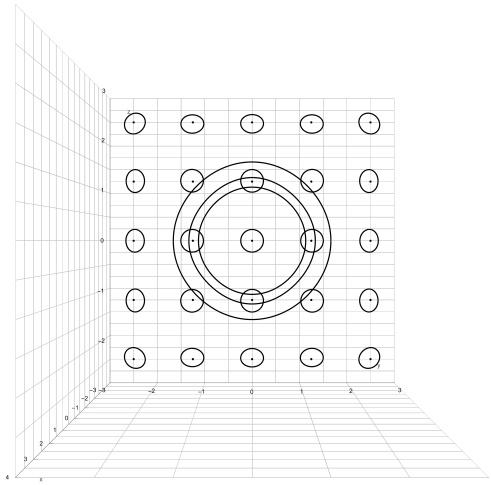

(a) Viewpoint 1

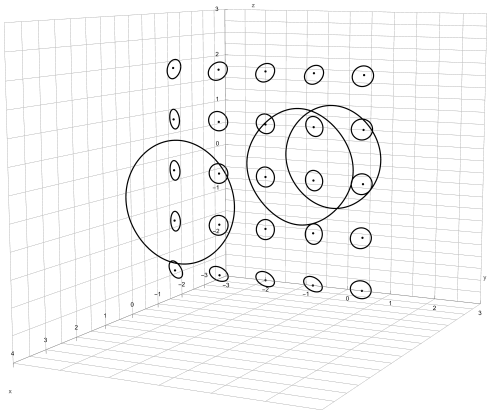

(b) Viewpoint 2

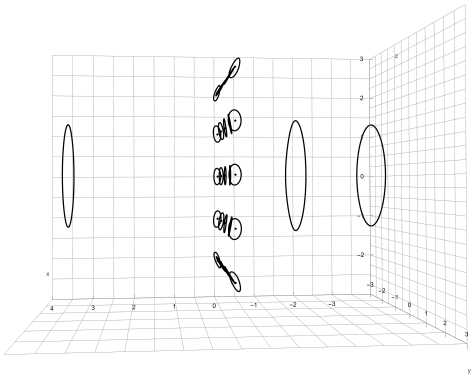

(c) Viewpoint 3

Figure 2.10: 25-interaction square lattice - nodal lines for the strength parameter $\alpha = -0.4$, the same for all of the 25 interactions and for perpendicular wave with momentum $k = 2(1, 0, 0)$

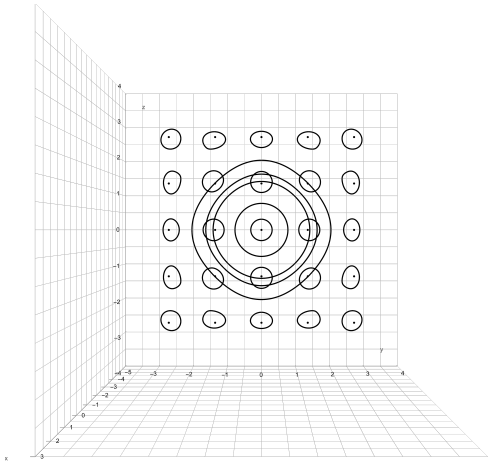

(a) Viewpoint 1

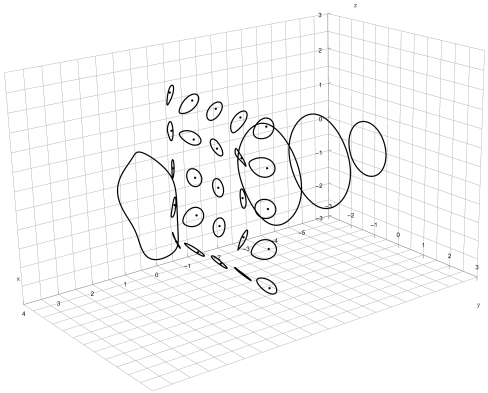

(b) Viewpoint 2

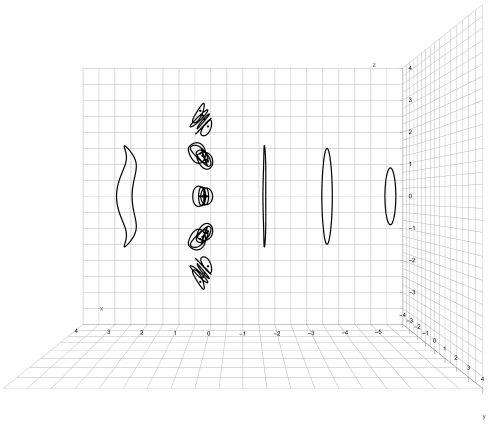

(c) Viewpoint 3

Figure 2.11: 25-interaction square lattice - nodal lines for the strength parameter $\alpha = -0.33$, the same for all of the 25 interactions and for perpendicular wave with momentum $k = 2(1, 0, 0)$

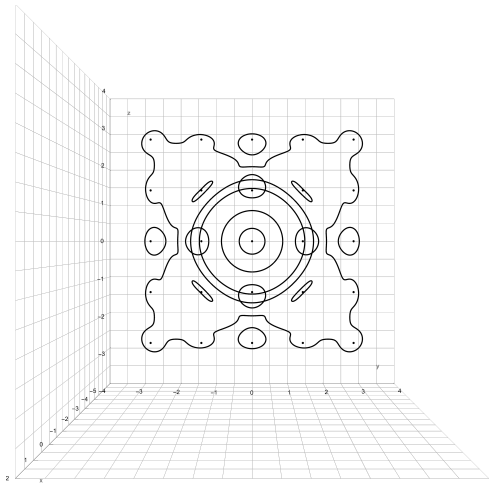

(a) Viewpoint 1

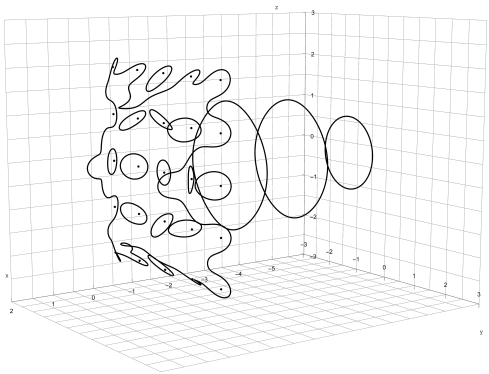

(b) Viewpoint 2

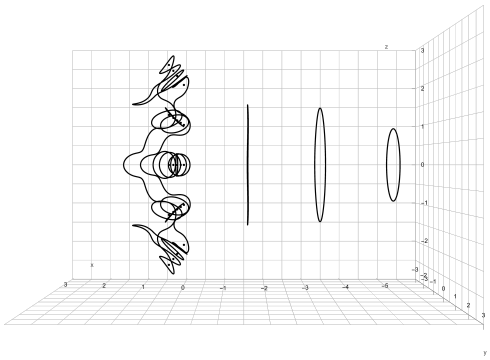

(c) Viewpoint 3

Figure 2.12: 25-interaction square lattice - nodal lines for the strength parameter $\alpha = -0.3$, the same for all of the 25 interactions and for perpendicular wave with momentum $k = 2(1, 0, 0)$

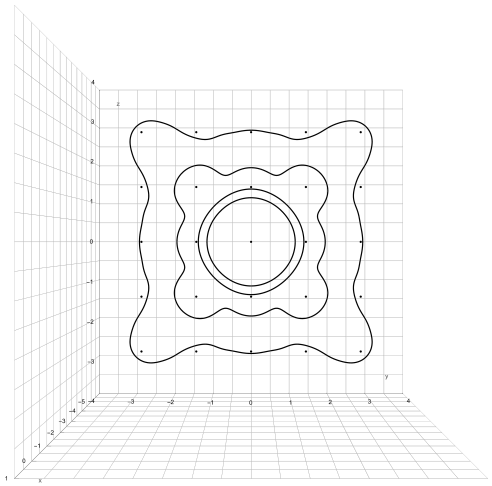

(a) Viewpoint 1

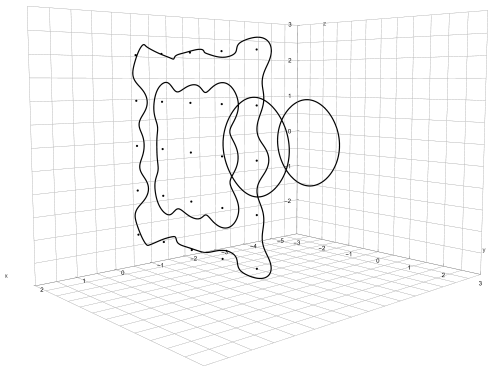

(b) Viewpoint 2

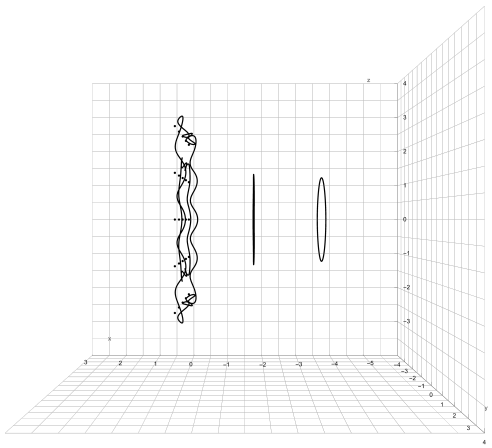

(c) Viewpoint 3

Figure 2.13: 25-interaction square lattice - nodal lines for the strength parameter $\alpha = -0.15$, the same for all of the 25 interactions and for perpendicular wave with momentum $k = 2(1, 0, 0)$

2.3.2 Wave perpendicular to 100 points forming a square lattice

Due to the occurrence of additional loops outside the vicinity of the lattice, we decided to examine a larger one to see if there is any connection between the grid size and the behaviour of these loops, and to estimate the behaviour of the infinite square lattice. Let us now consider a wave approaching the 10×10 grid perpendicularly, i.e. with momentum $\mathbf{k} = 2(1, 0, 0)$. The configuration changes mentioned here are not all of the changes for this case. We describe only some of the major ones that we observed, and therefore it is possible that we overlooked some of them, or that we did not consider them to be important at the time of the examination. Usually we mention critical values of α, when a new effect is perceptible (and, with the same precision, for lower value of α when it was not), or the interval at which the change occurs. Sometimes the resulting effect is obtained after a sequence of smaller changes (e.g. Fig. 2.16a did not happen all at once, the loops between the points arise gradually).

As in the previous situations, under a certain critical strength (here $\alpha_{crit} = -0.652$) there are only loops around each point of the lattice. Then, from $\alpha = -0.651$, loops appear progressively in front ($x < 0$) and behind ($x > 0$) the grid. In total, 18 loops appear gradually in front of the lattice ($x < 0$), including two concentric pairs of loops – at $x \approx -1.5$ and at $x \approx -3.0$ (specific values are given in Tab. 2.4). Especially notable are these two pairs of concentric loops (Fig. 2.15) which we did not observe in the 25 point case in section 2.3.1. The loops behind the lattice ($x > 0$) require a more detailed investigation, which will be summarized later. All of the loops in front of the lattice and one of the configurations behind the lattice can be seen in Fig. 2.15.

Concerning the behaviour of the loops behind the lattice, we will describe them in more detail in this paragraph. The loop, that appears for $\alpha = -0.501$ behind the lattice, at $x \approx 18.3$, moves with the growth of α closer to the lattice – for example for $\alpha = -0.334$ it is located around the interval $x \in (10, 11.5)$. For $\alpha = -0.339$, four loops behind the lattice appear (Fig. 2.14a), for $\alpha = -0.334$, two additional loops emerge – one spatial, extending for about $x \approx (0.5, 6.5)$, and the other one flat loop, slightly further from the lattice (Fig. 2.14b). For $\alpha = -0.330$ two flat loops, the furthest behind the lattice, disappear. Next, for $\alpha = -0.318$, one central loop can be observed (Fig. 2.14d) and then for $\alpha = -0.307$ the spatial loop and the four loops behind the lattice split into four perpendicular loops to the lattice. The rest joins the outside loop of the lattice (Fig. 2.15).

Again, there is a global effect in the form of two larger loops around this periodic set-up, for $\alpha \in (-0.180, -0.105)$. The loops inside these two global loops combine to form loops between points of the lattice for $\alpha \in (-0.175, -0.149)$ (Fig. 2.16a), and then they start to vanish. From $\alpha = -0.129$ in the vicinity of the lattice, only the two global loops around remain (Fig. 2.16b). These two loops, for $\alpha = -0.104$, join to create 4 oval loops, one on each side of the lattice, and 4 separate loops in the corners (Fig. 2.16c), thus consequently breaking this global effect. Later, for $\alpha = -0.057$, each of the 4 oval loops on the side of the grid splits into 3 loops (Fig. 2.16d).

Eventually, more loops appear (example in Fig. 2.17a). Some of them vanish later (example in Fig. 2.17b) for a moment, so that the configuration in the vicinity of the lattice consists of only 12 loops (Fig. 2.17c). Thereafter, the number of loops near the lattice increases (example in Fig. 2.17d) and later, for the last time, declines. Through these changes, the loops observed outside of the lattice gradually cease to exist – the last one ($x \approx -10$) for $\alpha = 0.109$. Finally, for $\alpha = 0.207$, the remaining loops in the lattice disappear and for $\alpha \in (0.207, \infty)$ there are no loops at all.

Specific values of α with the description of the corresponding change are listed in concise form in Tab. 2.4.

Strength α	Nodal line change
(-∞, -0.652)	Loops are only around each nodal point
-0.651	Loop at $x \approx -9.3$ appears
-0.641	Loop at $x \approx -10.8$ appears
-0.632	Loop at $x \approx -7.6$ appears
-0.618	Loop at $x \approx -12.4$ appears
-0.589	Loop at $x \approx -14.0$ appears
-0.557	Loop at $x \approx -15.6$ appears
-0.556	Loop at $x \approx -6.0$ appears
-0.528	Loop at $x \approx -17.3$ appears
-0.501	Loop at $x \approx 18.3$ appears
-0.491	Loop at $x \approx -18.9$ appears
-0.458	Loop at $x \approx -20.5$ appears
-0.423	Loop at $x \approx -22.0$ appears
-0.410	Loop at $x \approx -4.6$ appears
-0.386	Loop at $x \approx -23.7$ appears
-0.359	Two concentric loops at $x \approx -3.0$ appears
-0.356	Two concentric loops at $x \approx -1.5$ appears
-0.339	4 loops behind the grid ($x \geq 0$) appear
-0.337	Loop at $x \approx -25.3$ appears
-0.334	Behind the grid ($x \geq 0$) two loops appear. One spatial $x \in (0.5, 7)$, one flat at $x \approx 7$.
(-0.331, -0.330)	Loop created at $\alpha = -0.501$ and the next flat loop closer to the lattice disappear
-0.318	Small loop behind the grid ($x \geq 0$) appears
(-0.308, -0.307)	Spatial loop separates, creates 4 perpendicular loops and rest joins the outer lattice loop
(-0.301, -0.300)	Loops around outer points create one loop
(-0.180, -0.179)	Loops around fourth from the middle points create one loop
(-0.180, -0.179)	Loops in the inner 8×8 lattice start merging together, creating loops between the inner points
(-0.176, -0.175)	All of the loops of the inner, 8×8 lattice have loops between each other
(-0.130, -0.129)	Last loop in the inner 8×8 lattice disappears
(-0.105, -0.104)	Both loops around lattice connect
(-0.058, -0.057)	Loops on the side trisect
(0.108, 0.109)	Last loops outside of lattice disappear ($x \approx -10$)
(0.206, 0.207)	Last loops in lattice disappear
(0.207, ∞)	No nodal lines

Table 2.4: Some significant changes of nodal line configuration for 100 point interaction, square lattice perpendicularly approaching wave with momentum $\mathbf{k} = (2, 0, 0)$, depending on α. x-coordinates in the *nodal line change* column indicate approximate positions of points on the loops in the plane z = 0 for the specific α. With the growth of α, positions and shapes of the loops slightly change.

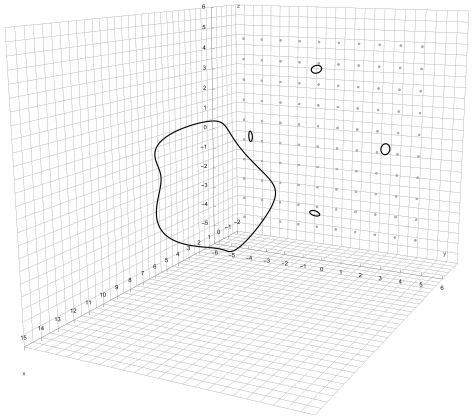

(a) $\alpha = -0.337$

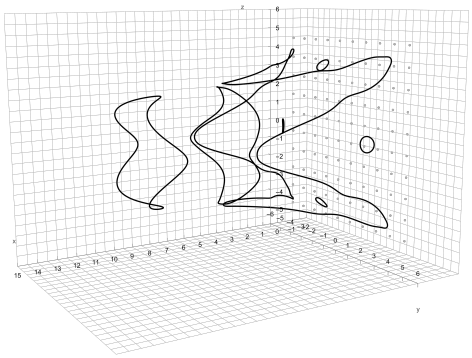

(b) $\alpha = -0.334$

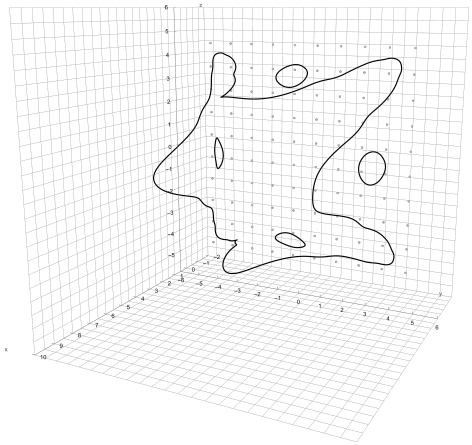

(c) $\alpha = -0.325$

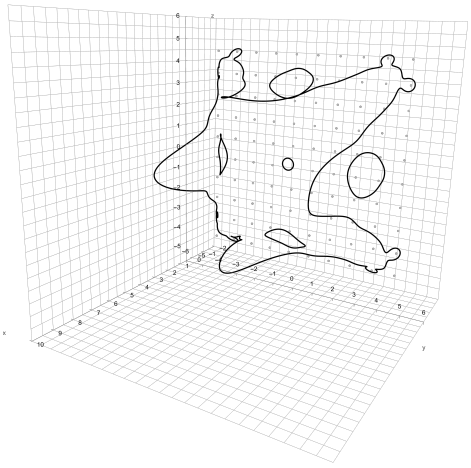

(d) $\alpha = -0.315$

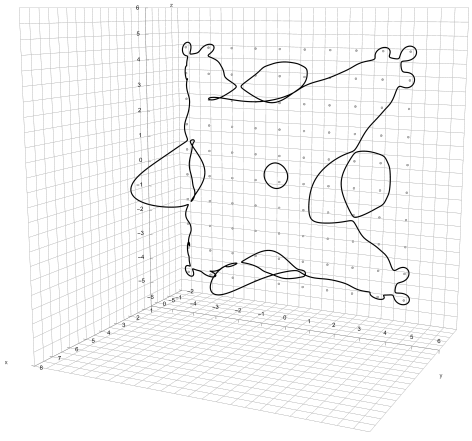

(e) $\alpha = -0.308$

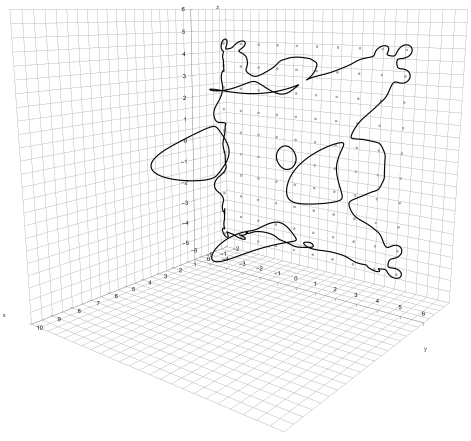

(f) $\alpha = -0.307$

Figure 2.14: 100-interaction square lattice - change of the nodal lines in front of the lattice (for positive x), depending on the strength parameter α, the same for all of the 100 interactions and for perpendicular wave with momentum $k = 2(1, 0, 0)$.

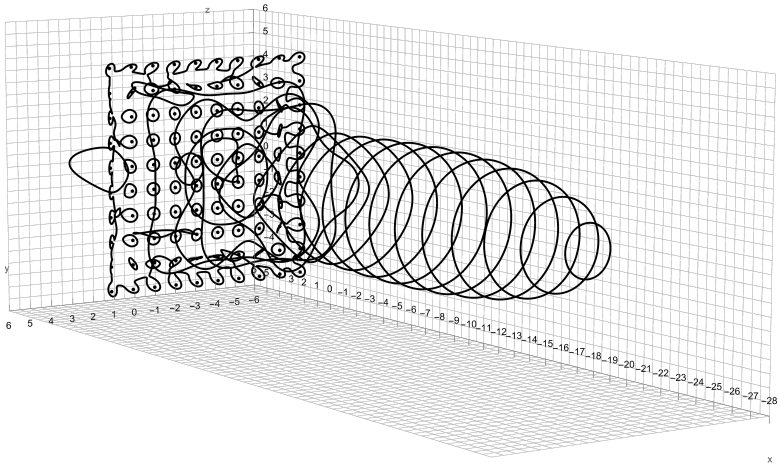

(a) Viewpoint 1

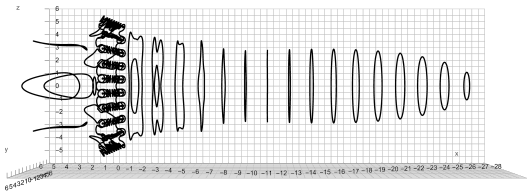

(b) Viewpoint 2

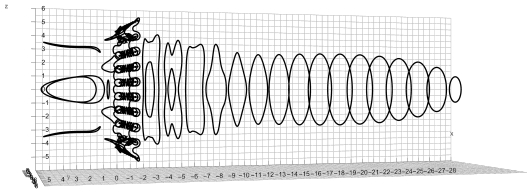

(c) Viewpoint 3

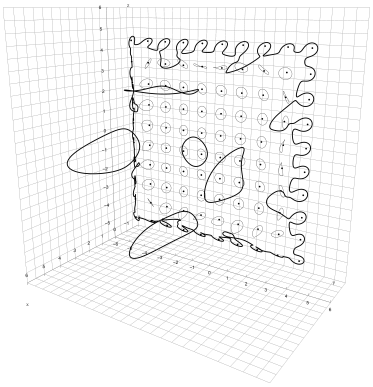

(d) Close-up of the part behind the lattice

Figure 2.15: 100-interaction square lattice - nodal lines for the strength parameter $\alpha = -0.3$, the same for all of the 100 interactions and for perpendicular wave with momentum $k = 2(1, 0, 0)$.
Representative example of all loops out of the lattice.

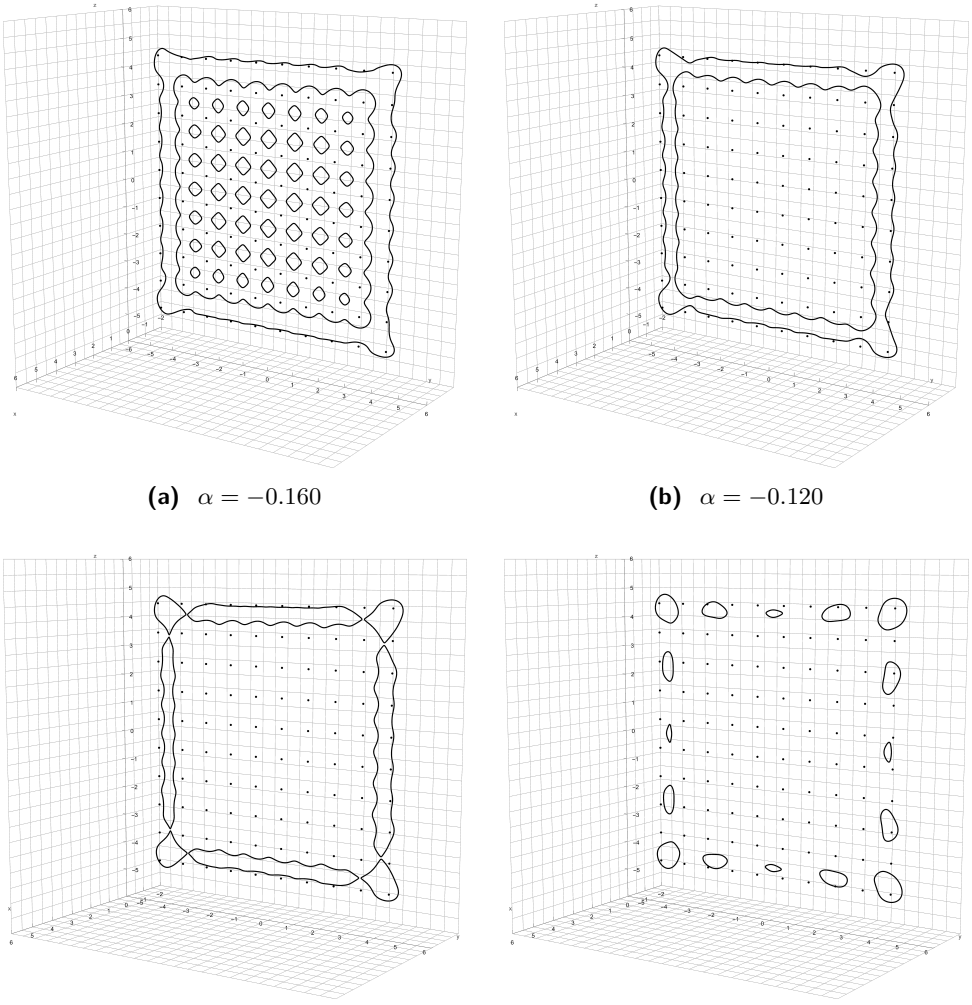

(a) $\alpha = -0.160$ **(b)** $\alpha = -0.120$

(c) $\alpha = -0.104$ **(d)** $\alpha = -0.05$

Figure 2.16: 100-interaction square lattice - nodal lines for the strength parameter the same for all of the 100 interactions and for perpendicular wave with momentum $k = 2(1, 0, 0)$, to show global effect. Here are plotted only loops in vicinity of the lattice.

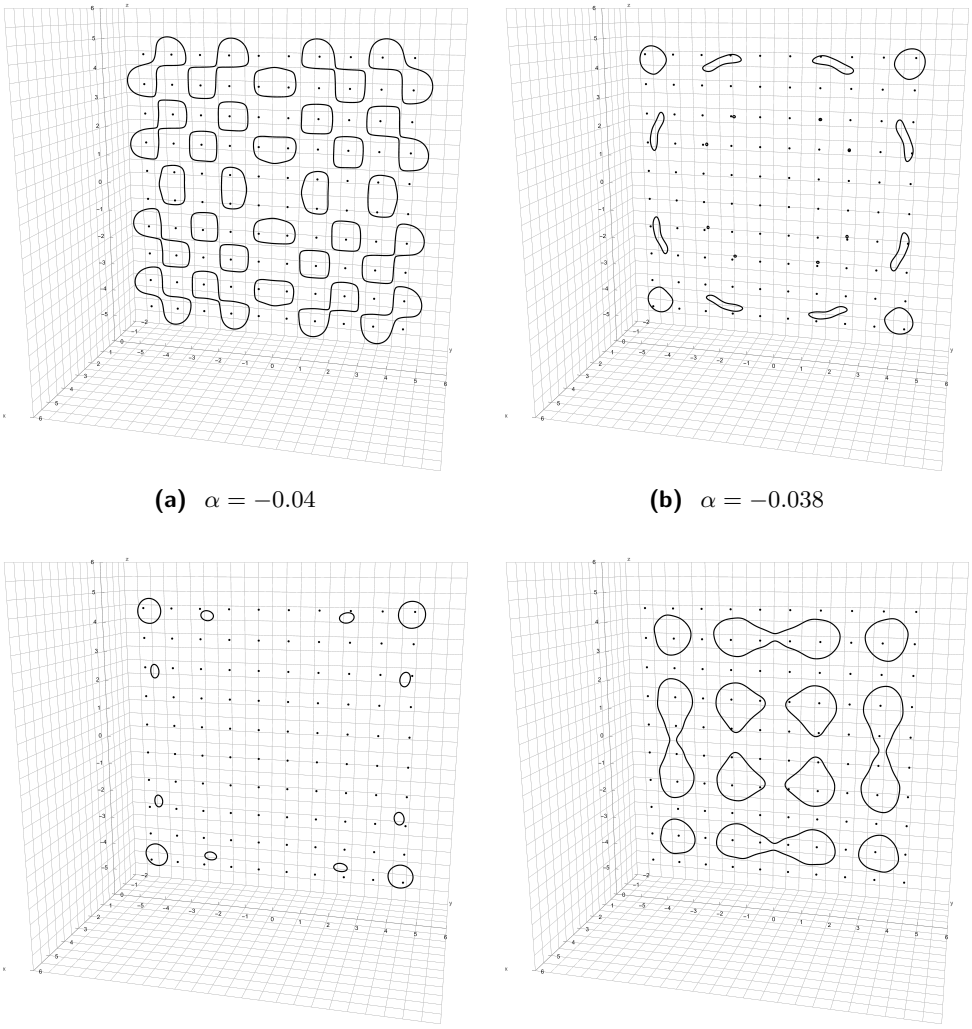

(a) $\alpha = -0.04$ **(b)** $\alpha = -0.038$

(c) $\alpha = 0$ **(d)** $\alpha = 0.1$

Figure 2.17: 100-interaction square lattice - change of the nodal lines in front of the lattice (for positive x), depending on the strength parameter α, the same for all of the 100 interactions and for perpendicular wave with momentum $k = 2(1, 0, 0)$.

2.3.3 Summary for a wave perpendicular to point interactions forming a square lattice

When examining the wave approaching a square lattice, we again discovered a global effect, in the form of a loop encircling all of the points of the grid, which in both cases (5×5 and 10×10) had one additional concentric loop in the lattice. Therefore, we have seen that in the case of the lattice, as opposed to the case of the point interactions on the line (section 2.2), additional loops can appear during the appearance of a global line.

Furthermore, in the 5×5 lattice, we first found loops that were not inside the lattice, but in front of the lattice as well as behind it (example in Fig. 2.11). To investigate the behaviour of a larger square lattice, we chose a 10×10 grid. As expected, the number of these loops increased, and we even saw concentric loops outside of the lattice, as well as loops that were almost perpendicular to the grid. In both cases, We also observed that the last loop outside the lattice disappear earlier (for lower α) than the last loop inside the lattice. Some of the more important configuration changes are summarised in Tab. 2.3 for 5×5 grids and Tab. 2.4 for 10×10 grids.

With regard to both of these two global effects in the infinite lattice, we conjecture that they would remain closed, unlike in the on line configuration (section 2.2). However, we would have to use a different approach if we wanted to prove this assumption.

2.4 Hexagonal lattice with 6 points on each side

In this section we will study a hexagonal lattice, with 6 points on each side (i.e. 91 points in total) and with the same spacing of 1 between the neighbouring points (Fig. 2.18), as was used previously. We will again consider a wave with momentum $k = 2(1, 0, 0)$ – perpendicularly approaching the hexagonal lattice.

Again here we find critical value of alpha $\alpha_{crit} = -0.624$. Below this value only loops around each of the point interactions occur. Same as in the previous case of the square lattice in section 2.3.2, we observe two concentric loops in front of the lattice. For a moment, there are also two almost concentric (there are in a close proximity in terms of the x-coordinate) loops behind the lattice.

The behaviour of the loops behind the lattice ($x > 0$) is discussed here in more detail. For $\alpha = -0.575$, the loop at $x \approx 14.5$ appears and as the parameter α increases, this particular loop moves closer to the lattice. For $\alpha = -0.405$ at $x \approx 4.2$ an additional set of 6 symmetrically (with respect to the hexagonal symmetry of the lattice) placed loops emerge (Fig. 2.19a). These six loops join for $\alpha = -0.396$ to form two concentric loops (Fig. 2.19b). For $\alpha = -0.389$ a new set of 6 symmetrically placed independent loops at $x \approx 1.2$ appear (Fig. 2.19d) only for them to be later connected at $\alpha = -0.364$ with the closer loop from the pair (created for $\alpha - 0.396$) (Fig. 2.19e). For $\alpha \in (-0.354, -0.318)$ a small loop at $x \approx 0.8$ is observed. Finally, we can perceive more loops, even though some of them later disappear again. For $\alpha = -0.179$, there is only one loop behind the lattice (Fig 2.20d).

The last loop outside the lattice ($x \approx -8.1$) vanishes for $\alpha = 0.122$ (Fig. 2.21a). And later, for $\alpha = 0.152$, the last group consisting of 6 loops in the lattice disappears (Fig. 2.21b), resulting in the case with zero loops for all larger strength parameters α.

Compared with the 10×10 square lattice case (section 2.3.2), we found no diametrically distinct results, although the nodal lines slightly differ due to different geometry of the points. The creation of multiple concentric loops outside the lattice, which we first observed in the larger square lattice, occurs here as well (examples in Figs. 2.19, 2.20).

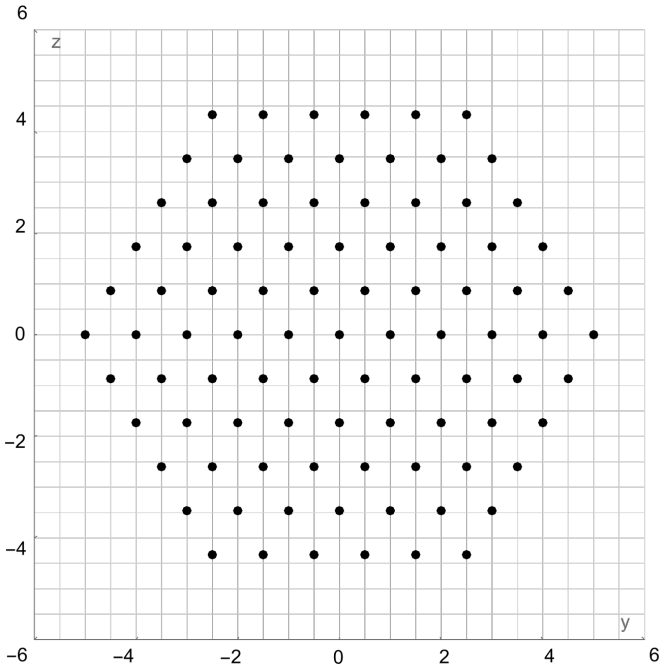

Figure 2.18: Configuration of the hexagonal lattice with 91 points

Strength α	Nodal line change
(-∞, -0.624)	Loops are only around each nodal point
-0.623	Loop at $x \approx -7.7$
-0.621	Loop at $x \approx -9.3$
-0.599	Loop at $x \approx -10.9$
-0.588	Loop at $x \approx -6.0$
-0.575	Loop at $x \approx 14.5$
-0.566	Loop at $x \approx -12.5$
-0.527	Loop at $x \approx -14.1$
-0.521	6 symmetrically placed loops at $x \approx -3.0$
-0.509/-0.508	6 loops join to create two concentric loops at $x \approx -3.0$
-0.504	Loop at $x \approx -4.5$
-0.484	Loop at $x \approx -15.8$
-0.478	6 symmetrically placed loops at $x \approx -1.4$
-0.467/-0.466	Two concentric loops at $x \approx -1.4$ from 6 loops joined together
-0.435	Loop at $x \approx -17.4$
-0.405	6 symmetrically placed loops at $x \approx 4.2$
-0.397/-0.396	Two concentric loops at $x \approx 4.2$ from 6 loops joined together
-0.389	6 symmetrically placed loops at $x \approx 1.2$
-0.368	Loop at $x \approx -19.0$
-0.365/-0.364	6 loops connect with one of the concentric loops at $x \approx 1.2$
(-0.354–0.318)	Loop at $x \approx 0.8$
-0.326/-0.325	Outer loops connect to create one big loop
-0.189/-0.188	Loops around the second most outer points connect and create one big loop
(0.121, 0.122)	Last loops outside of lattice disappear ($x \approx -8$)
(0.151, 0.152)	Last loops in lattice disappear
(0.152, ∞)	No nodal lines

Table 2.5: Some significant changes of nodal line configuration for interaction of 91 points in hexagonal lattice, perpendicularly approached by a wave with momentum $\mathbf{k} = (2, 0, 0)$, depending on α. x-coordinates in the *nodal line change* column indicate approximate positions of points on the loops in the plane z = 0 for the specific α. With the growth of α, positions and shapes of the loops slightly change.

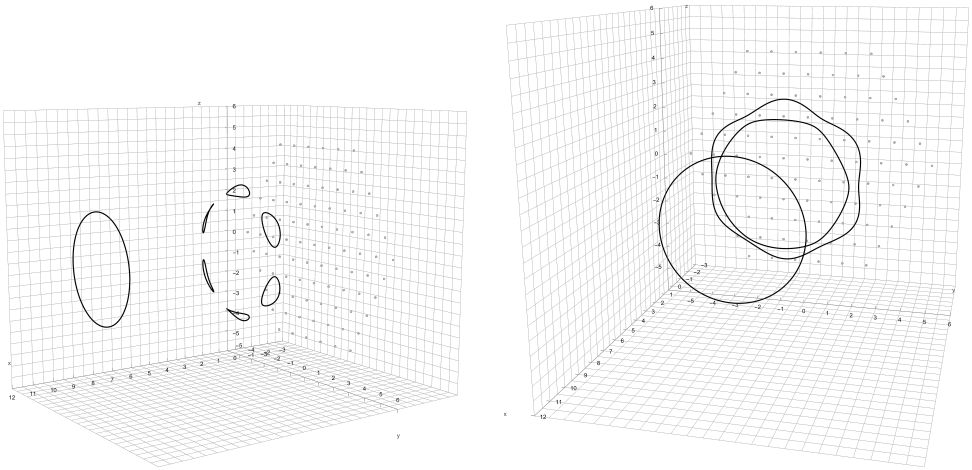

(a) $\alpha = -0.4$ **(b)** $\alpha = -0.394$

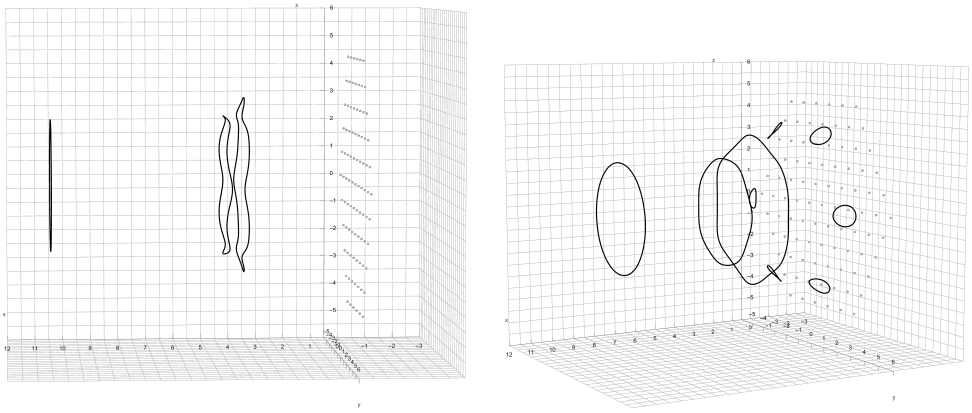

(c) $\alpha = -0.394$ side view **(d)** $\alpha = -0.380$

Figure 2.19: 91-interaction hexagonal lattice, the strength α the same for all the interactions, perpendicular wave with momentum $k = 2(1, 0, 0)$.
Change of the nodal lines in front of the lattice ($x > 0$), depending on $\alpha \in (-0.405, -0.330)$.

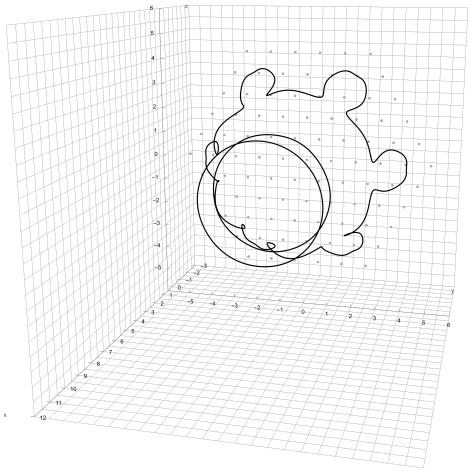

(e) $\alpha = -0.360$

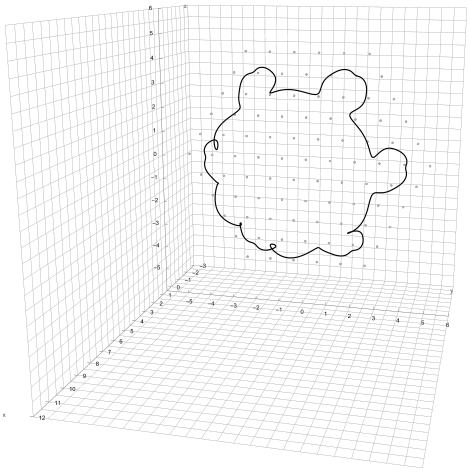

(f) $\alpha = -0.356$

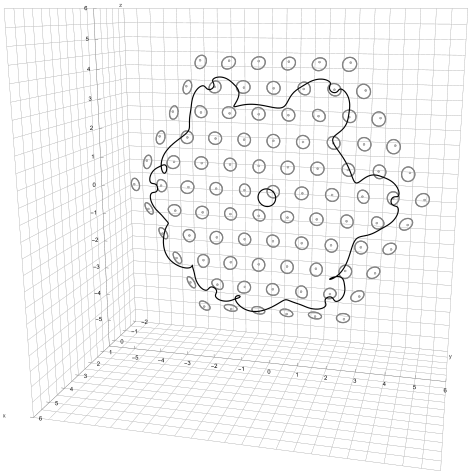

(g) $\alpha = -0.350$

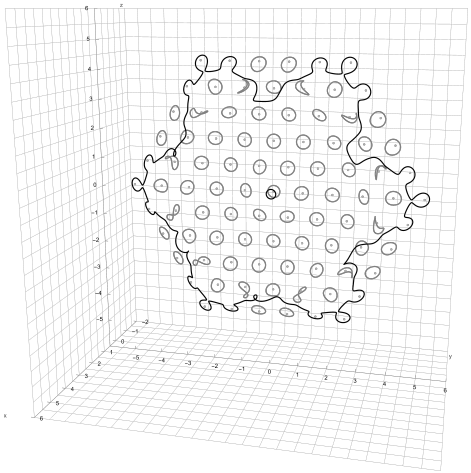

(h) $\alpha = -0.330$

Figure 2.19: 91-interaction hexagonal lattice, the strength α the same for all the interactions, perpendicular wave with momentum $k = 2(1, 0, 0)$. Change of the nodal lines in front of the lattice ($x > 0$), depending on $\alpha \in (-0.405, -0.330)$.

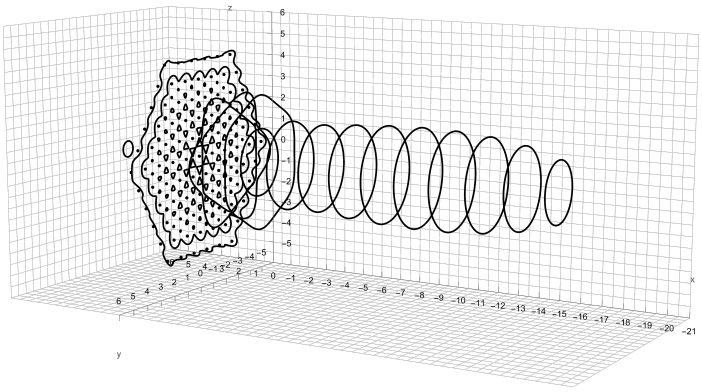

(a) Viewpoint 1

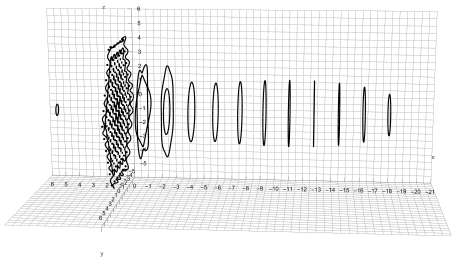

(b) Viewpoint 2

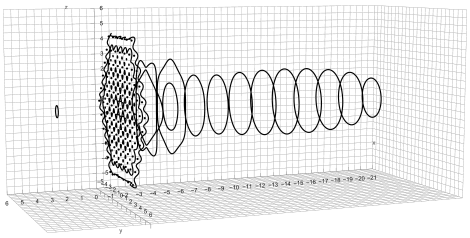

(c) Viewpoint 3

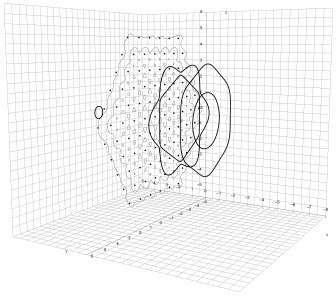

(d) Close-up of the neighbourhood of the lattice

Figure 2.20: Nodal lines for the strength parameter $\alpha = -0.179$, the same for all of the 91 interactions on hexagonal lattice, and for perpendicular wave with momentum $k = 2(1, 0, 0)$.
For this α there already remains only 17 out of 18 loops in front $x < 0$ loops, the farthest one disappeared.

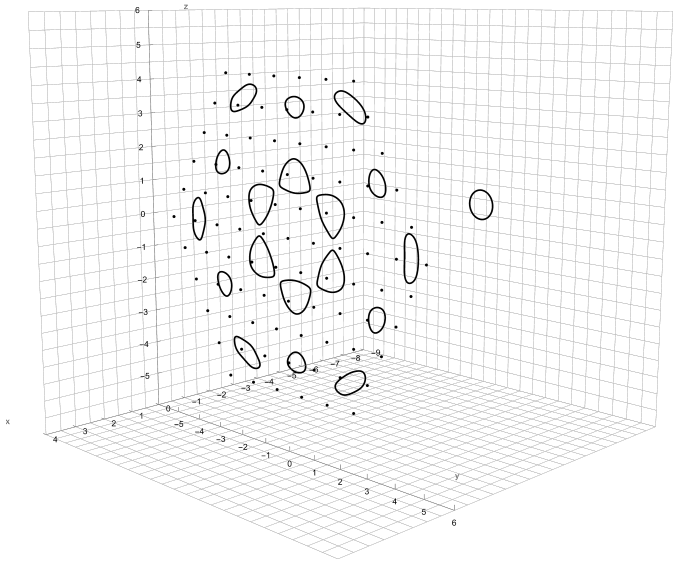

(a) $\alpha = 0.11$

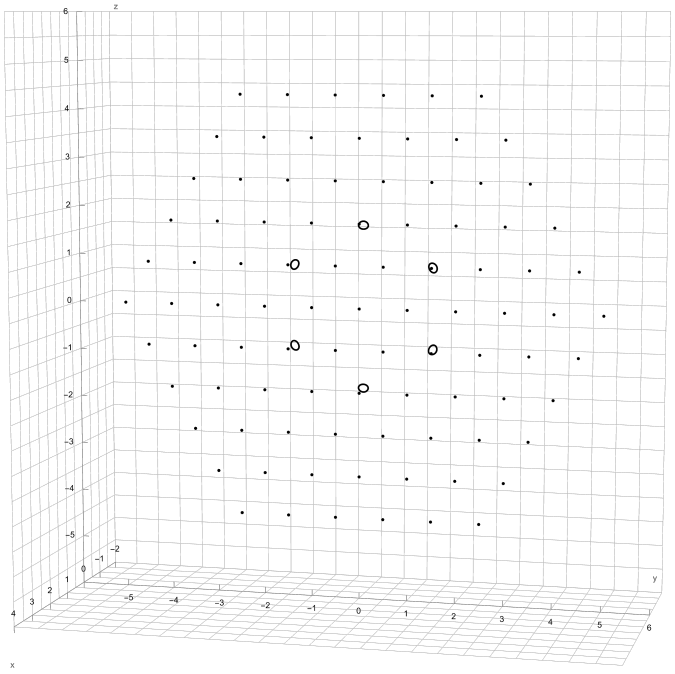

(b) $\alpha = 0.15$

Figure 2.21: Nodal lines for the strength parameter $\alpha = -0.179$, the same for all of the 91 interactions on hexagonal lattice, and for perpendicular wave with momentum $k = 2(1, 0, 0)$.
Configurations before all lines, in front of/behind and in the lattice respectively, disappear.

Conclusion

In this thesis, we began by summarising the theory behind the point interaction (section 1), using the textbook [2].

In the following section we focused on the periodic systems of point interactions (section 2). We have found out, that even in the simplest systems (such as equidistant, same strength, point interactions on a line), a global effect in the form of a closed loop around all the interactions appear (Fig. 2.3). In other words, one loop encircling all the point interactions is created instead of a set of multiple separate loops around each interaction (Fig. 2.2). This effect is dependent on the strength of the interactions and the angle, under which the particle approaches this configuration. We created table 2.1 of configuration changes, depending on the strength of the interactions. We discovered (section 2.2.2), that a borderline angle, where this global effect ceases to appear, is $8°$ ($\pm$ $0.5°$). It also gives a hint that global patterns may exist in scattering on truly infinite systems. Regarding the scatter on points on the line, it seems that the global lines might take form of two "parallel" lines that are not closed. To test this assumption, however, we would have to use different methods.

Finally we tried a more complex periodic system - a lattice, with a perpendicularly approaching particles and the same strength for all the interactions. Starting with a rather small 5×5 square lattice (section 2.3.1), we observed, apart from similar effects to those around the point interactions on the line (Figs. 2.12, 2.13), another global effect in the form of centered loops in front of and behind the lattice (Figs. 2.10, 2.11, 2.12, 2.13). To find out how these additional loops change, we tried a larger 10×10 lattice (section 2.3.2),

where more loops appeared outside the designed lattice. For both of these configurations we made tables with some of the significant changes (Tabs. 2.3; 2.4). In order to verify that these outside loops are not connected just with a square lattice, we formed a similarly sized 91 point hexagonal lattice. While investigating this proposed structure, we observed that the shape of the loops changed according to the symmetry of this case. Nevertheless, we still observed larger loop around the lattice (Fig. 2.20), as well as loops in front of and behind the lattice (Figs. 2.19, 2.20, 2.21a). We conjecture that in infinite lattices of this type all the nodal lines would remain closed.

Bibliography

[1] A. A. Abrikosov. The magnetic properties of superconducting alloys. *Journal of Physics and Chemistry of Solids, vol. 2, number 3*, pages 199–208, 1957.

[2] S. Albeverio, F. Gesztesy, R. Høegh-Krohn, and H. Holden. *Solvable Models in Quantum Mechanics, 2nd edition.* International series of monographs on physics. American mathematical society, 2005.

[3] J. Blank, Pavel Exner, and M. Havlíček. *Hilbert Space Operators in Quantum Physics, 2nd edition.* Springer Netherlands, Dordrecht, 2008.

[4] T. Chiueh, T. P. Woo, H-Y Jian, and H-Y Schive. Vortex turbulence in linear schrödinger wave mechanics. *Journal of Physics B: Atomic, Molecular and Optical Physics, vol. 44, number 11*, page 115101, May 2011.

[5] B. S. Deaver and W. M. Fairbank. Experimental evidence for quantized flux in superconducting cylinders. *Physical Review Letters, vol. 7, Issue 2*, pages 43–46, 1961.

[6] R. Doll and M. Näbauer. Experimental proof of magnetic flux quantization in a superconducting ring. *Physical Review Letters, vol. 7, Issue 2*, pages 51–52, 1961.

[7] P. Exner and P. Šeba. Probability current tornado loops in three-dimensional scattering. *Physics Letters A, vol. 245*, pages 35–39, 1998.

[8] V. L. Ginzburg. On superconductivity and superfluidity (what i have and have not managed to do), as well as on the 'physical minimum' at the beginning of the 21st century. *ChemPhysChem, vol. 5, number 7*, pages 930–945, 2004.

[9] D. M. Gitman, I. V. Tyutin, and B. L. Voronov. *Self-adjoint extensions in quantum mechanics: general theory and applications to Schrödinger and Dirac equations with singular potentials*. Progress in mathematical physics, vol. 62. Springer Science & Business Media, 2012.

[10] G. Jaeger. The Ehrenfest classification of phase transitions: Introduction and evolution. *Archive for History of Exact Sciences, vol. 53, number 1*, pages 51–81, May 1998.

[11] K. Jörgens. Wesentliche selbstadjungiertheit singulärer elliptischer differentialoperatoren zweiter ordnung. *Mathematica Scandinavica, vol. 15*, pages 5–17, 1964.

[12] L. D. Landau. On the theory of phase transitions. I. *Phys. Z. Sowjet., vol. 11*, page 26, 1937.

[13] M. Reed and B. Simon. *Methods of Modern Mathematical Physics. II: Fourier analysis, self-adjointness*. Elsevier, 1975.

[14] G. I. Taylor and A. E. Green. Mechanism of the production of small eddies from large ones. *Proceedings of the Royal Society of London. Series A - Mathematical and Physical Sciences, vol. 158, number 895*, pages 499–521, 1937.

[15] E.V. Thuneberg. *Encyclopedia of condensed matter physics*, pages 128–133. Elsevier, Academic Press, 2005.